AFRL-RV-PS-
TR-2014-0133

HIGH-RESOLUTION REGIONAL PHASE ATTENUATION MODELS OF THE IRANIAN PLATEAU AND SURROUNDING REGIONS

Eric Sandvol, et al.

Department of Geological Science
University of Missouri
Columbia, MO 65211

3 March 2014

Final Report

AIR FORCE RESEARCH LABORATORY
Space Vehicles Directorate
3550 Aberdeen Ave SE
AIR FORCE MATERIEL COMMAND
KIRTLAND AIR FORCE BASE, NM 87117-5776

DTIC COPY

NOTICE AND SIGNATURE PAGE

Using Government drawings, specifications, or other data included in this document for any purpose other than Government procurement does not in any way obligate the U.S. Government. The fact that the Government formulated or supplied the drawings, specifications, or other data does not license the holder or any other person or corporation; or convey any rights or permission to manufacture, use, or sell any patented invention that may relate to them.

This report was cleared for public release by the 377 ABW Public Affairs Office and is available to the general public, including foreign nationals. Copies may be obtained from the Defense Technical Information Center (DTIC) (http://www.dtic.mil).

AFRL-RV-PS-TR-2014-0133 HAS BEEN REVIEWED AND IS APPROVED FOR PUBLICATION IN ACCORDANCE WITH ASSIGNED DISTRIBUTION STATEMENT.

//SIGNED//	//SIGNED//
Robert Raistrick	Glenn M. Vaughan, Colonel, USAF
Project Manager, AFRL/RVBYE	Chief, Battlespace Environment Division

This report is published in the interest of scientific and technical information exchange, and its publication does not constitute the Government's approval or disapproval of its ideas or findings.

REPORT DOCUMENTATION PAGE

Form Approved
OMB No. 0704-0188

1. REPORT DATE *(DD-MM-YYYY)*	**2. REPORT TYPE**	**3. DATES COVERED** *(From - To)*
03-03-2014	Final Report	01 March 2011 to 28 February 2014

4. TITLE AND SUBTITLE
High-Resolution Regional Phase Attenuation Models of the Iranian Plateau and Surrounding Regions

5a. CONTRACT NUMBER
FA9453-11-C-0235

5b. GRANT NUMBER

5c. PROGRAM ELEMENT NUMBER
62601F

6. AUTHOR(S)
Eric Sandvol, Ayoub Kaviani, Rengin Gok, Wenfei Ku, and Xueyang Bao

5d. PROJECT NUMBER
1010

5e. TASK NUMBER
PPM00009371

5f. WORK UNIT NUMBER
EF004194

7. PERFORMING ORGANIZATION NAME(S) AND ADDRESS(ES)
Department of Geological Science
University of Missouri
Columbia, MO 65211

8. PERFORMING ORGANIZATION REPORT NUMBER

9. SPONSORING / MONITORING AGENCY NAME(S) AND ADDRESS(ES)
Air Force Research Laboratory
Space Vehicles Directorate
3550 Aberdeen Avenue SE
Kirtland AFB, NM 87117-5776

10. SPONSOR/MONITOR'S ACRONYM(S)
AFRL/RVBYE

11. SPONSOR/MONITOR'S REPORT NUMBER(S)
AFRL-RV-PS-TR-2014-0133

12. DISTRIBUTION / AVAILABILITY STATEMENT
Approved for public release; distribution is unlimited. (377ABW-2014-0485 dtd 07 Jul 2014)

13. SUPPLEMENTARY NOTES

14. ABSTRACT

The objective of this project is to construct regional wave (Pg, Sn, and Lg) attenuation models for the crust and upper mantle throughout the Iranian plateau and surrounding regions. This research should increase ray path coverage of critical areas and help to create robust regional phase amplitude and attenuation models. We have combined our Iranian data set with our existing Middle Eastern Lg waveform database. These two data sets, combined, give us reasonably good coverage of the northern Middle East. We have created a catalog of seismic events in and around Iran with reliable source spectra as well as tested regional phase attenuation maps for the Zagros and Iranian plateau. We have developed an Sn attenuation model using two station measurements of Q for regional phase Sn (0.1 to 0.5 Hz) and for high frequency Sn (0.5 to 2 Hz). We have also processed Pg waveforms in order to obtain robust estimates of Qp in the crust within the Iranian plateau. For most of the phases we see moderately high attenuation within the plateau and less attenuation along the Zagros mountains. This project is the first to use two station and reverse two station methods to measure attenuation of phases such as Pg and Sn.

15. SUBJECT TERMS
variational analysis, adjoint method, Data assimilation

16. SECURITY CLASSIFICATION OF:			**17. LIMITATION OF ABSTRACT**	**18. NUMBER OF PAGES**	**19a. NAME OF RESPONSIBLE PERSON**
a. REPORT	**b. ABSTRACT**	**c. THIS PAGE**			Robert Raistrick
Unclassified	Unclassified	Unclassified	Unlimited	62	**19b. TELEPHONE NUMBER** *(include area code)*

Standard Form 298 (Rev. 8-98)
Prescribed by ANSI Std. 239.18

This page is intentionally left blank.

Table of Contents

Figures

This page is intentionally left blank.

1. SUMMARY

The objective of this project is to construct and validate regional wave (Pg, Sn, and Lg) attenuation models for the crust and upper mantle throughout the Iranian plateau and surrounding regions. This research should increase ray path coverage of critical areas and help to create robust regional phase amplitude and attenuation models. We have recently combined our Iranian data set that with our existing Middle Eastern Lg waveform database. Together, these two data sets give us reasonably good coverage of the northern Middle East. We have created a catalog of seismic events in and around Iran with reliable source spectra as well as tested regional phase attenuation maps for the Zagros and the Iranian plateau. Although much of our project focused on Lg we have also developed a frequency dependent Sn attenuation model using two station Q measurements for long period Sn (0.1 to 0.5 Hz) and for high frequency Sn (0.5 to 2 Hz). We have processed Pg waveforms in order to obtain robust estimates of Qp in the crust within the Iranian plateau. The long period frequency band Sn is very similar to what Barron and Priestley, 2009 used (0.2 for long period, 1 Hz for high frequency) for the frequency dependent propagation Sn across Tibet. We have compared our various Q models with other measurements of amplitude and velocity variation to help understand the source of regional phase attenuation in this complex tectonic environment. In addition to Sn and Lg we have also developed a Pg attenuation model for the Iranian plateau. We present this model for the first time in this report. In parallel with the two station studies we have developed coda 1-D corrections for the Iranian plateau which should help to better determine reliable source spectra for seismic events within Iran.

2. INTRODUCTION

2.1 Background on Lg

The Lg-wave and its coda typically constitute the most prominent phase observed on regional-distance seismograms recorded from crustal events traveling over continental paths (Molnar and Oliver, 1969). Lg waves can be treated either as a superposition of higher mode surface waves (Knopoff, et al., 1973; Kennett, 1984) or as multiply reflected shear waves trapped within the crust (Bouchon, 1982, Campillo, 1990). Lg propagates entirely within the crust and retains strong amplitudes over long regional distances and therefore provides a good measure of path-averaged crustal attenuation and velocity of seismic shear waves (Mitchell, 1997). In active tectonic regions such as the Tibetan and Turkish-Iranian plateaus, the Lg wave is highly attenuated (e.g., Kadinsky-Cade et al., 1981, Xie et al., 2002; Zor et al., 2007; Bao et al., 2011a and 2011b). The reduction in Lg wave amplitudes in tectonically active regions is most likely caused by high intrinsic attenuation related to the presence of fluids in cracks, scattering along tectonic faults, the presence of partial melt, or rapid variations in the thickness of the waveguide (e.g., Campillo, 1990, Mitchell, 1997).

Crustal attenuation studies have application both to practical objectives such as earthquake magnitude calibration, seismic hazard assessment, and seismic monitoring

and to studies addressing the evolution and deformation of the continental crust. We report here on the results of the investigation of Lg wave attenuation and velocity across the northern Middle-East, including the Turkish-Iranian plateau, the Zagros mountain range, and the south Caspian basin. This study is one of the first to measure both velocity and Q in order to correlate the two measurements.

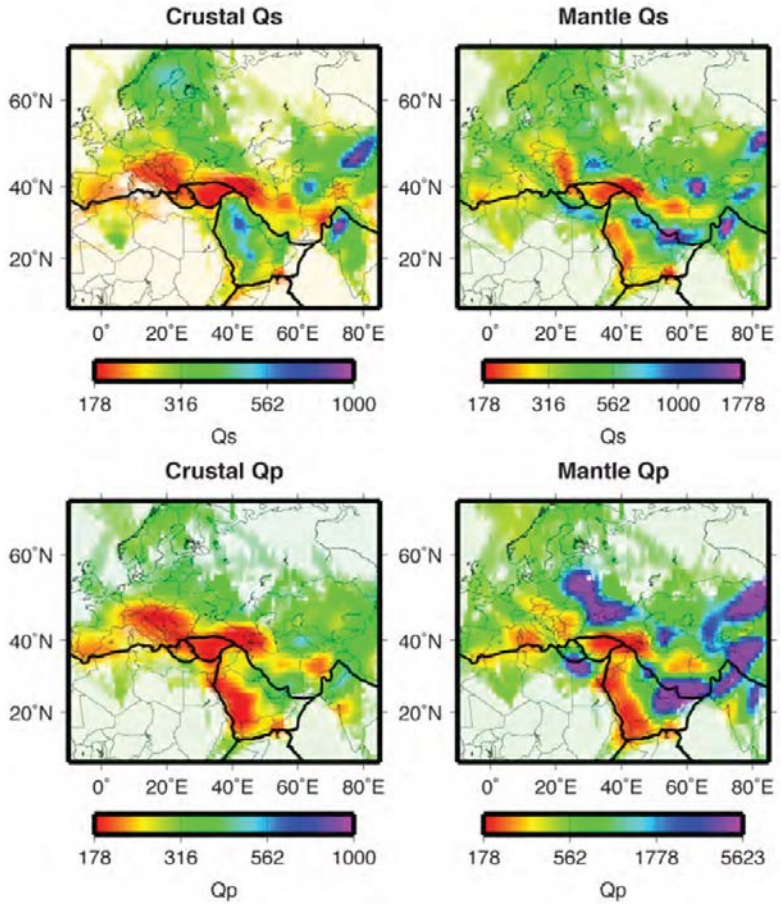

Figure 1. A map showing a three dimensional Q model tomographically derived from crustal phases Pg and Lg (Qp and Qs respectively) and from mantle phases Pn and Sn (Pasaynos et al., 2009).

2.2 Tectonic and Geophysical Setting

The first important attempt to map upper mantle attenuation with Sn was Molnar and Oliver, 1969, followed by Kadinsky-Cade et al (1981) (Figures 1 and 2); both studies showed very weak Sn propagation in the Iranian-Turkish Plateau. The same study demonstrates that Lg is also absent or weak on the seismograms with paths crossing the Plateau and across the south Caspian Sea. Later studies by Mitchell et al (1997), Rodgers et al (1997) and Cong and Mitchell (1998) confirmed the same results. The more detailed studies by Sandvol et al (2001), Gök et al (2003) and Al-Damegh et al (2006) indicate Lg blockage across the Bitlis Suture and the Zagros fold and thrust belt and weak Lg and Sn propagation in most parts of the Iranian-Turkish Plateau (Baumgardt, 2001). These studies indicate coincidence of the regions of Sn inefficient propagation or blockage with regions of low Pn velocities (e.g. Al-Lazki et al, 2003). The teleseismic tomography study of the upper mantle velocity structure by Kaviani et al (2007) revealed strong velocity contrast between the Arabian and Eurasian lithospheres in the Zagros collision zone with relatively lower speed lithosphere beneath central Iran.

The correlation of the regions of high attenuation and low velocities with the regions of the Cenozoic volcanism leads many authors to conclude that the lithosphere beneath the Iranian-Turkish Plateau is probably hot and thin. The south Caspian Block is usually considered as having an oceanic type crust. The previous studies showed weak propagation of Lg for the paths crossing the block. The poor ray coverage, however, prevented unambiguous conclusions regarding Lg propagation and its implications for crustal type.

All of the above mentioned studies have been performed on a regional scale that had poor resolution in the Iranian Plateau. High resolution mapping of the Turkish Plateau was obtained using data collected at the local networks (Zor et al., 2007; Gök et al., 2010). The Iranian Plateau is another important piece of the puzzle that is needed for a high resolution map of the crustal and upper mantle attenuation in the Middle-East.

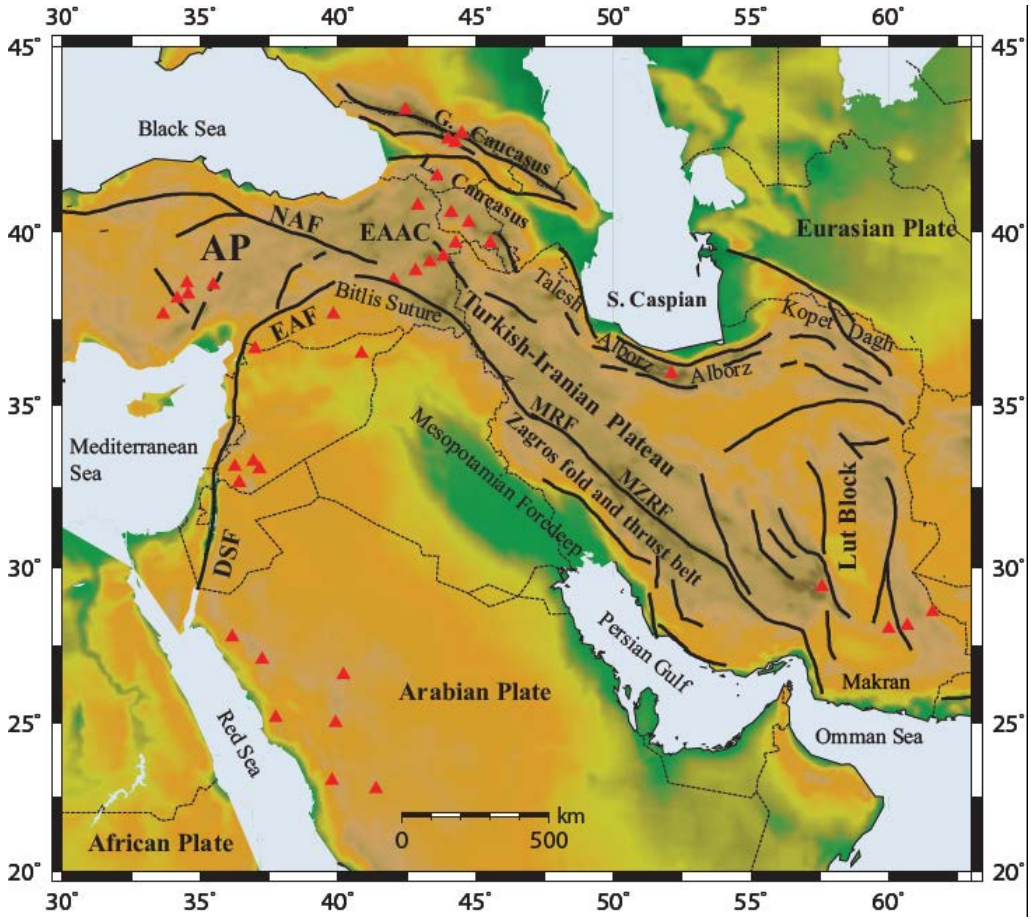

Figure 2. A topographic map superimposed with the major tectonic features across the Middle East. The major faults are depicted with black solid lines. The main continental boundary fault zones and tectonic settings are abbreviated on the map and described here. The red triangles present the location of quaternary volcanoes. The dashed thin lines indicate political boundaries. AP: Anatolian Plateau, EAAC: East Anatolian Accretionary Complex, NAF: Northern Anatolian Fault, EAF: Eastern Anatolian Fault, DSF: Dead Sea Fault, MZRF: Main Zagros Reverse Fault, MRF: Main Recent Fault.

The Iranian Plateau is being squeezed between two regions of stable shield-type continental crust, Arabia from the south and Turkmenia from the north (Figure 2). It has been accommodating the Arabia-Eurasian convergence since Early Cenozoic by crustal shortening in the main mountain belts (Zagros, Alborz and Kopet-Dag) and by strike-slip movements along the border between the micro-blocks constituting central Iran. The current state of the Plateau is the result of a long history of tectonic evolution begun by separation of the central Iranian microblocks (CIMB) from the Afro-Arabian mega-continent in the Paleozoic, followed by closure of the Paleo-and then Neo-Tethys and re-arrangement and amalgamation of the CIMB in the Mesozoic and finally by collision of the Arabia and CIMB in late Cretaceous-Early Cenozoic. This long history has created different tectonic provinces in Iran, each comprising one part of the Plateau (Figure 3). On the other hand, the Zagros collision zone as the youngest continental collision in the world provides a unique natural laboratory to investigate the early states of the continental lithosphere in a tectonically active zone.

The Zagros thrust zone and the distributed fault zones within the Iranian plateau mark a young continental collision zone that is undergoing 20 mm/yr of shortening (Jackson and McKenzie, 1984) including active oceanic subduction and distributed strike slip faulting. The Zagros extend for 1500 km along the Iran-Iraq border and are the result of the Miocene collision of the Arabian plate with the Eurasian plate (e.g. Stocklin, 1968). This collision zone is further characterized by a 2.0 km topographic high (Iranian plateau) with corresponding crustal seismicity that indicates that this region is still actively deforming although there is strong evidence that for the vast majority of the Zagros and Iranian plateau there is no seismicity beneath 20 km (Maggi et al., 2001).

GPS results from McClusky et al. (2000) indicate that the lithosphere in the Lesser Caucasus is possibly being extruded to the east. Focal mechanisms suggest that the distributed strike slip faulting that is prevalent in eastern Turkey extends into the northwestern Iranian plateau, although there is poor correlation between surface geologic features and crustal earthquakes (Berberian, 1995). There is evidence of right lateral strike slip movement on the main recent fault along the northern portion of the Zagros thrust and fold belt (Tchalenko and Braud, 1974; Talebian and Jackson, 2002). Focal mechanisms near the Caspian Sea coast clearly indicate that the Talesh and Alborz Mountains are overthrusting the Caspian Basin, which is also consistent with the movement of the lesser Caucasus to the east (Priestley et al., 1994).

The geological evolution of that segment of the Middle East which includes the Zagros fold and thrust belt and the Iranian plateau can be characterized in part by accretionary tectonics where tectonostratigraphic terranes of different origins are now juxtaposed (Figure 3). Although the origin of most of these terranes can be traced back to continental margins of the Eurasian or the Afro-Arabian plate, others have oceanic characteristics (e.g., ophiolites) and must have been accreted segments of Tethyan Ocean crust placed onto the continental margins (e.g., Dewey and Bird, 1970; Moores and Vine, 1971; Coleman, 1981; Michard et al., 1984; Lippard et al., 1986; Peters et al., 1991).

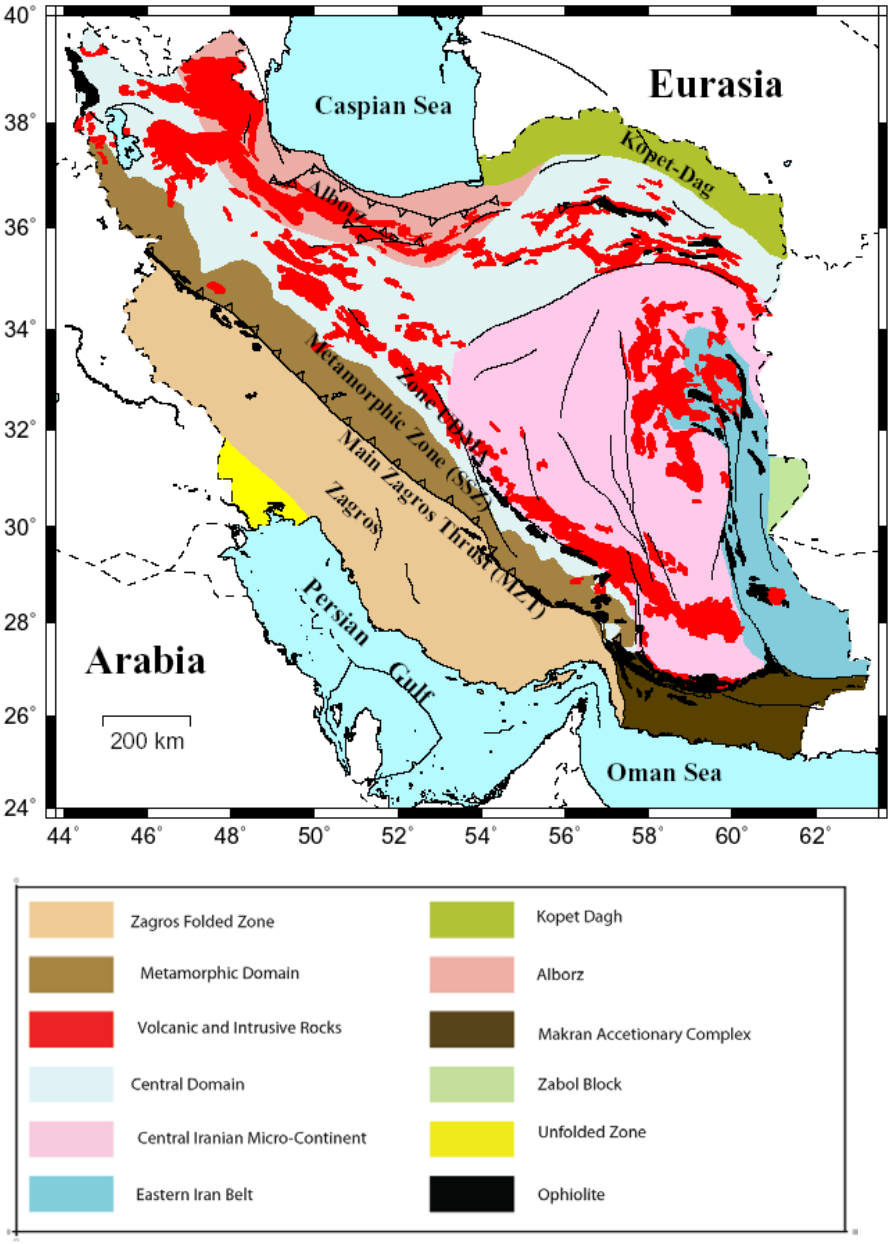

Figure 3. Index map showing main tectonic elements of Iran, modified from the structural map of NGDIR (National Geoscience Database of Iran), http://www.ngdir.ir

In addition to the Khoy ophiolite in NW Iran which has Ar/Ar crystallization ages of 158-160 Ma (Ghazi et al., 2001) and bio-chronostratigraphic ages of middle to late Cretaceous (i.e., Albian, Coniacian and Campanian-Maasterictian from Pessagno et al., 2002), there are other subduction/collision-related geological features. For example, Sabalan (ca. 4800 m) has been determined to be a Quaternary composite volcano and consists of primarily alkaline (trachyte, dacite, latite with minor basalt) volcanic rocks (Berberian and King, 1981) suggesting the presence of extensive crustal melting. Sahand (ca. 3800 m) is another composite volcano in the area which is of late Miocene- early Pliocene age and is made up of calc-alkaline volcanic rocks (almost entirely dacite with minor andesite

plugs) (Berberian and King, 1981). Berberian and King suggest that both of these volcanoes are collision related, similar to Supan and Ararat located within the eastern Anatolian plateau to the west.

2.3 Prior Attenuation Studies in the Middle East

Cong and Mitchell (1998) imaged the lateral variations in the Lg coda quality-factor at 1 Hz (Q_0) and its frequency dependence in the Middle-East and showed that Lg coda Q_0 ranges between 150 and 300 over the Turkish and Iranian Plateaus. They observed relatively higher Q_0 values (300-450) over the Arabian shield and platform regions but the values are lower than the typical values expected for stable shield regions. The large-scale Lg coda attenuation studies over the Eurasia by Mitchell et al., (1997) and Mitchell et al., (2008) confirm the same findings, although the resolution of the images in these latter studies are too low to reveal detailed features of Lg attenuation in such complex regions as the northern Middle-East where small-scale lateral variations in the crustal properties across the different tectonic settings are expected. Sandvol et al., (2001) and Al-Damegh et al., (2004), by studying the propagation efficiency of regional waves, observed that the Lg wave is inefficient or blocked across the Bitlis suture and Zagros belt. They interpret that the Lg blockage results from a major lateral change in the crustal waveguide. Zor et al., (2007) imaged very low Lg Q_0 (60-300) within the Turkish Plateau. Pasyanos et al., (2009) inverted Lg amplitudes from broad-band seismograms for frequency-dependent Lg Q across the Middle-East. The interstation separation used by Pasyanos et al., (2009) is relatively large and thus the resolution of their tomographic images is low relative to our high resolution models. Nevertheless, the main features presented by Pasyanos et al., (2009) are consistent with our findings with the highest Lg attenuation found in eastern Turkey, moderate Lg Q in central Iran and the Zagros and the lowest Lg attenuation beneath the Arabian Shield. Pasyanos et al., (2009) also observed that the Lg attenuation beneath the S. Caspian Basin is moderate. Bao et al., (2011b) observe that the variation of Pg Q_0 and its frequency dependence over the northern Middle East is well correlated with that of Lg Q_0. To date there have been very few crustal scale Lg attenuation studies over the Iranian Plateau. Kadinsky-Cade et al., (1981), through analysis of Lg waves over a small number of paths across the Turkish and Iranian plateaus, report that Lg propagates efficiently over the Iranian Plateau but is inefficient across the Zagros belt and is blocked along the paths across the south Caspian. Rodgers et al., (1997) also confirm the same results.

In this paper we report on an integrated tomographic models for Pg, Lg, and Sn Q over the Turkish-Iranian plateau and the Zagros. The results are obtained by analysis of a large data set gathered from a dense network of broad-band and short-period stations operated over the northern Middle East during the last decade.

3. TECHNICAL APPROACH

3.1 Data

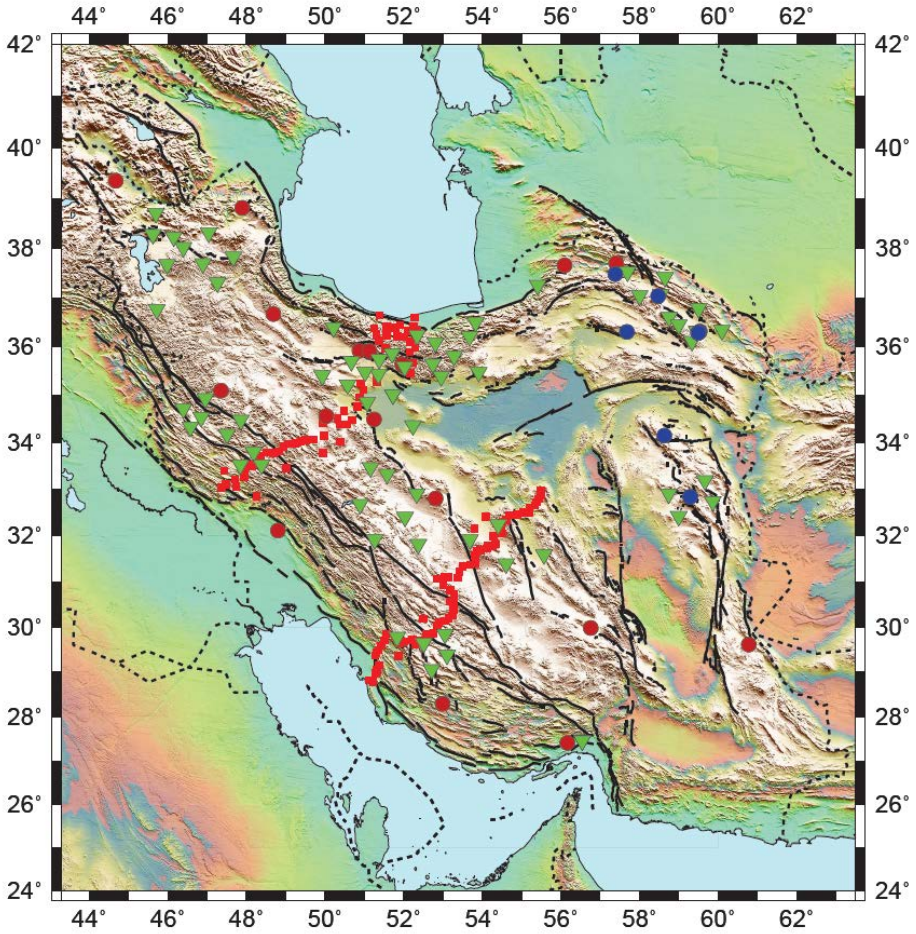

Figure 4. A regional topographic map showing the broadband (circles) and short-period stations (triangles) from all of the temporary and permanent networks that have been deployed across the Iranian plateau and Zagros Mountains. These stations are nearly all three component**.**

The available data provides an unprecedented opportunity to study the crustal and uppermost mantle attenuation in this intact region. The current compiled data set consists of up to 10 years of recorded waveforms collected by 74 permanent short-period stations operated by the Institute of Geophysics of Tehran University (IGTU), up to 4 years of continuous recording from 17 permanent broad-band stations operated by the International Institute of Earthquake Engineering and Seismology (IIEES), up to 8 years of records from 6 broad-band stations of the Khorasan Seismological Network in northeast Iran operated by the Earthquake Research Center of the Ferdowsi University of Mashad (EQRC). These networks were equipped with a combination of short-period and broad-band sensors and operated in continuous mode (Figure 4).

We processed all of these data in order to measure reverse two station Q in order to construct a robust attenuation model for the Iranian plateau. We assigned propagation efficiencies to each regional seismogram, windowed the Lg and Pg regional phases, used these windows to calculate two station Q values, and then applied the Reverse Two Station approach to all of the data.

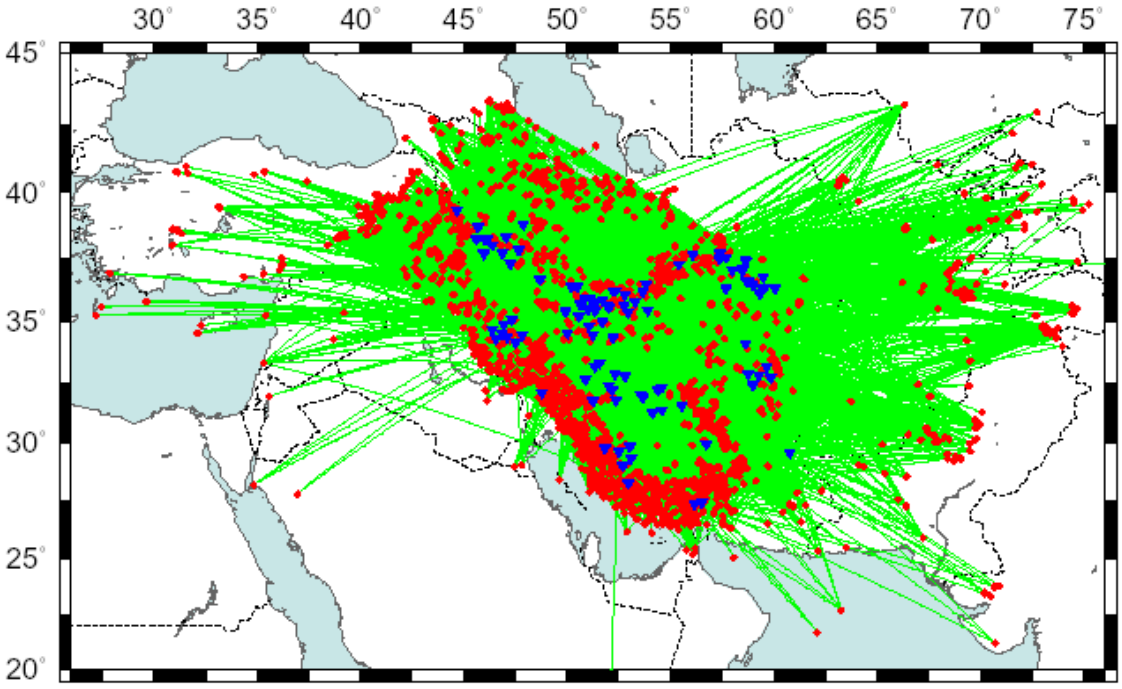

Figure 5. A map of local and regional earthquakes recorded by both temporary and permanent stations in Iran during period of 2006-2009. The green dots are the earthquake epicenters and the blue inverted triangles are seismic stations.

The final number of event-station pairs is 20358 ray paths from 2453 regional events of magnitude greater than 4.0. This very large data set is essential for using our technique because the two-station method requires contemporaneous coverage of the stations (Figure 5).

3.2 Methodology Review

The amplitude of a seismic wave may be described by an exponential attenuation equation that accounts for both geometric spreading and attenuation,

$$A_{ij}(f) = I_i(f) S_{Si}(f) S_j(f) G(\Delta_{ij}) \exp\left(-\frac{\pi f \Delta_{ij}}{vQ(f)}\right) \qquad (1)$$

where A is the observed amplitude between source (indices j) and receiver (indices for a wave of frequency f recorded at distance Δ. Here, I_i is the instrument response, S_j is the source amplitude, S_{Si} is the site amplification response, and v is the wave group speed. The Geometric spreading is defined as the following:

$$G(\Delta) = \frac{1}{\Delta^m} \tag{2}$$

For cylindrical spreading m should be 0.5 and for spherical spreading m is 1.0. When dispersion is accounted for these can increase by up to 0.3 depending on signal bandwidth. We assume this function is frequency independent, however, this may be a poor assumption in many cases and these differences will be mapped into our effective Q or more specifically the scattering component of our effective Q. Spreading relations are important but poorly documented and must be given explicit attention in attenuation problems. The attenuation quality factor, Q, can be assumed to be frequency dependent, $Q=Q_0 f^{\eta}$ with Q_0 being the attenuation quality factor at 1 Hz, f the wave frequency, and η describing the frequency dependence. Values for Q_0 and η depend on the type of wave used but generally η lies between zero and one. This equation does not account for radiation pattern, focusing, or anisotropic effects. However, with good azimuthal coverage, these effects should average out. Both Q and amplitude tomography methods are based on this equation, with appropriate modifications.

The TSM was presented by Mitchell (1980) and has been widely used (e.g., Nuttli, 1986). Xie and Mitchell (1990) and uses the assumption of spreading such as that shown in equation 2 and that $Q(f)=Q_0^{-\eta}$:

$$(1-\eta)\ln f - \ln Q_0 = \frac{v}{\pi(d_j - d_i)} \ln\left(\frac{A_i(f) I_j(f) d_i^m}{A_j(f) I_i(f) d_j^m}\right). \tag{3}$$

where $d_j-d_i=\Delta$. The real situation for applying the TSM is more complicated because the perfect alignment geometry is typically not obtainable, especially for passive seismic experiments. In practice, event to station paths differ by a small angle $\delta\theta$. A detailed analysis on this angle has been presented by Xie et al. (2004). Systematic errors could be introduced into Q_0 and η values determined by the TSM because of effects of attenuation out of the path and anisotropic source radiation patterns. These errors can be minimized if a threshold value $\delta\theta_{\max}$ is used to limit the angle $\delta\theta$. Xie et al. (2004) used a $\delta\theta_{\max}$ of ±15° in their study, which had been estimated by Der et al. (1984). Xie et al. (2004) also derived an equation to minimize an error related to the variation of inter-station distance at 1 Hz. This equation (A14 in Xie et al., 2004) is reorganized here:

$$\frac{\delta Q}{Q^2} = \frac{v}{\pi f} \frac{1}{(d_j - d_i)} \delta x \,. \tag{4}$$

where d_j-d_i is the inter-station distance, δQ_0 is the error in the measured Q_0, and δx is the total error which is unaccounted for in equation (3) which assumes an ideal geometry and 1 D structure. In this study, we follow Xie (2004) by setting $\delta\theta_{\max}$ to 15° and δx smaller than 0.4. Also, the equation indicates that to reduce the Q error, it is preferable to maximize the inter-station distance.

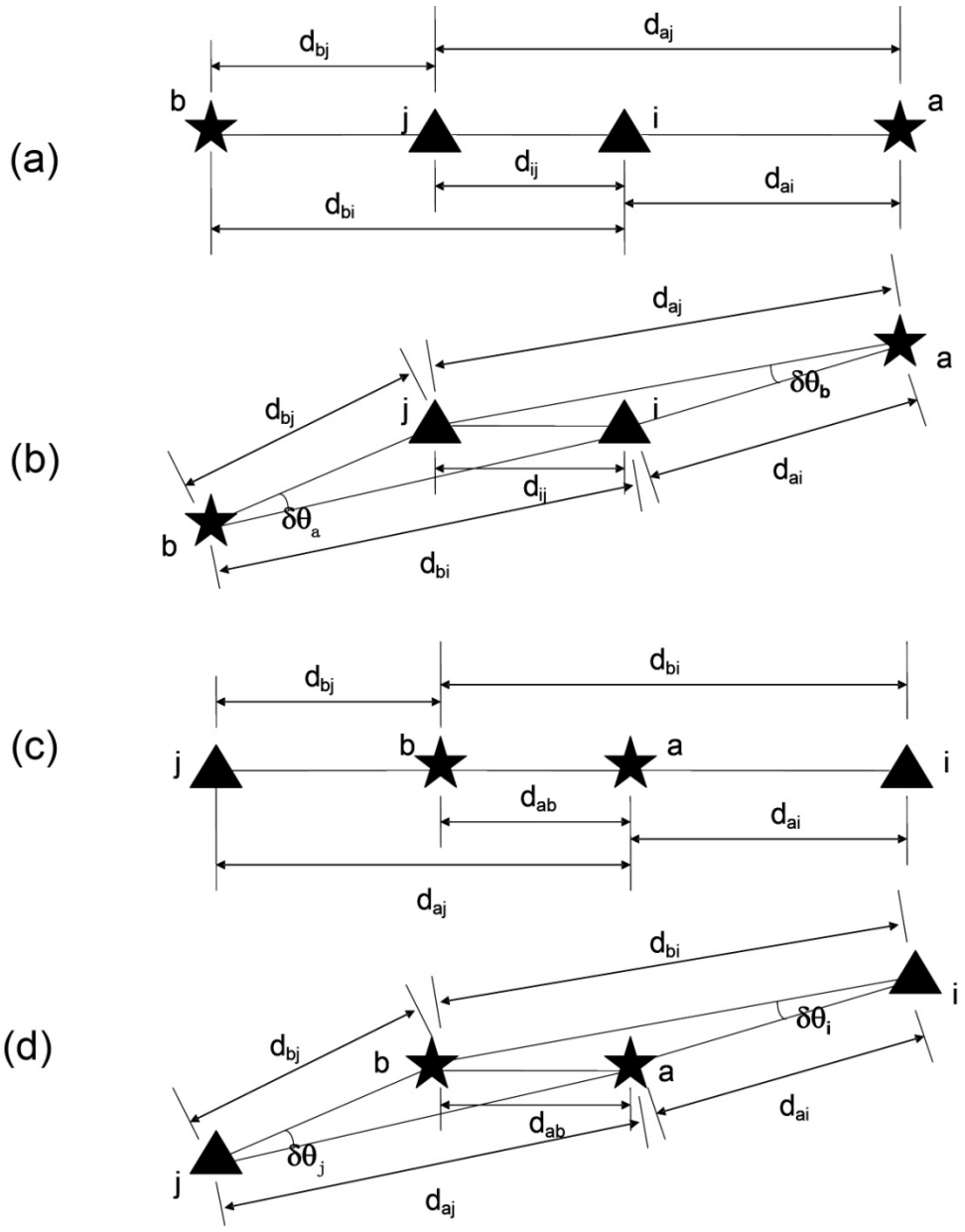

Figure 6. (a) and (b): Schematic drawing of the geometry of RTS including (a) the ideal situation where the source *a* (star in the right), the station *i* and *j* (triangles), and source *b* (star in the left) are aligned along a great circle, and (b) the more common situation where the azimuth difference angles from sources *a* and *b* to the stations are denoted by $\delta\theta_a$ and $\delta\theta_b$ respectively. (c) and (d): Schematic drawing of the geometry of RTE including (c) the ideal situation where the station *i* (triangle in the right), the sources *a* and *b* (stars), and station *j* (triangle in the left) are aligned along a great circle, and (d) the more common situation where the azimuth difference angles from stations *i* and *j* to the events are denoted by $\delta\theta_i$ and $\delta\theta_j$ respectively.

The main disadvantage of the TSM is caused by the remaining instrument response I and neglected site response $S_S(f)$ The instrument responses are only theoretically identical for stations with identical seismometers and data loggers. In practice, instrument calibration is commonly impossible during deployment, which also

does not preclude the influence of various time-varying uncalibrated instabilities on the recorded amplitude. It is also difficult to guarantee the operability of calibration of all instruments. The site effects have been suggested to have strong lateral variations and are likely associated with shallow geological structures, especially in tectonically active zones (Wald and Allen, 2007; Meunier et al., 2008; Pasyanos et al., 2009). Therefore, the site effects independent of instruments can contaminate the measurements of Q if we use the TSM. It is probably an over-simplification to assume the complicated instrument response and site response with a merely theoretically consistent model of instrument response and a neglected site response.

The RTM was suggested to avoid the effects of neglected S_S terms and inaccurate I terms in the TSM by involving one more event. The RTM was initially suggested by Chun et al. (1987). Figure 6 shows the geometry of the RTM including its two cases: the Reverse Two Station (RTS) paths and Reverse Two Event (RTE) paths. The ideal case for RTS is that both events are aligned with the inter-station path, and requires the four epicentral distances involved to be within a regional distance range. In such a situation, we use A_{ai}, A_{aj}, A_{bi}, and A_{bj} to denote spectral amplitudes of *Lg* recorded at stations i and j for events a and b, and d_{ai}, d_{aj}, d_{bi}, and d_{bj} the corresponding distances. The four spectral amplitudes can be expressed as:

$$
\begin{aligned}
A_{ai}(f,d_{ai}) &= S_a(f)R_a(f,\varphi)I_i(f)S_{Si}(f)G_{ai}(d_{ai})\exp\left[-\frac{\pi f d_{ai}}{vQ_i}\right] \\
A_{aj}(f,d_{aj}) &= S_a(f)R_a(f,\varphi)I_j(f)S_{Sj}(f)G_{aj}(d_{aj})\exp\left[-\frac{\pi f d_{aj}}{vQ_j}\right] \\
A_{bi}(f,d_{ai}) &= S_b(f)R_b(f,\varphi)I_i(f)S_{Si}(f)G_{bi}(d_{bi})\exp\left[-\frac{\pi f d_{ai}}{vQ_i}\right] \\
A_{bj}(f,d_{bj}) &= S_b(f)R_b(f,\varphi)I_j(f)S_{Sj}(f)G_{bj}(d_{bj})\exp\left[-\frac{\pi f d_{bj}}{vQ_j}\right].
\end{aligned}
\tag{5}
$$

If A_{ai} is divided by A_{aj} and A_{bi} is divided by A_{bj}, we get (note the exponents are negative):

$$
\begin{cases}
\dfrac{A_{ai}}{A_{aj}} = \dfrac{S_a}{S_a}\dfrac{R_a}{R_a}\dfrac{I_i}{I_j}\dfrac{S_{Si}}{S_{Sj}}\dfrac{G_{ai}}{G_{aj}}\exp\left(\dfrac{\pi f d_{aj}}{v_j Q_j}-\dfrac{\pi f d_{ai}}{v_i Q_i}\right) = \dfrac{I_i}{I_j}\dfrac{S_{Si}}{S_{Sj}}\dfrac{G_{ai}}{G_{aj}}\exp\left(\dfrac{\pi f d_{aj}}{v_j Q_j}-\dfrac{\pi f d_{ai}}{v_i Q_i}\right) \\
\dfrac{A_{bi}}{A_{bj}} = \dfrac{S_b}{S_b}\dfrac{R_b}{R_b}\dfrac{I_i}{I_j}\dfrac{S_{Si}}{S_{Sj}}\dfrac{G_{bi}}{G_{bj}}\exp\left(\dfrac{\pi f d_{bj}}{v_j Q_j}-\dfrac{\pi f d_{bi}}{v_i Q_i}\right) = \dfrac{I_i}{I_j}\dfrac{S_{Si}}{S_{Sj}}\dfrac{G_{bi}}{G_{bj}}\exp\left(\dfrac{\pi f d_{bj}}{v_j Q_j}-\dfrac{\pi f d_{bi}}{v_i Q_i}\right)
\end{cases}.
\tag{6}
$$

Like the TSM, we assume that the velocity structure is one-dimensional and apparent Q values are identical for the path between stations i and j, and thus we have not included the event subscripts (a and b). We divide the two ratios in (5), substitute, and obtain

$$\frac{A_{ai}A_{bj}}{A_{aj}A_{bi}} = \left(\frac{d_{ai}d_{bj}}{d_{aj}d_{bi}}\right)^{-m} \exp\left[\frac{\pi f}{vQ}\left(d_{aj} - d_{ai} - d_{bj} + d_{bi}\right)\right]. \tag{7}$$

where all of the Q parameters above are a function of frequency and m is the exponent from equation 2. Therefore, the inter-station (between *i* and *j*) apparent 1/*Q* value can be derived as

$$\frac{1}{Q} = \frac{v}{\pi f\left(d_{aj} - d_{ai} - d_{bj} + d_{bi}\right)} \ln\left[\frac{A_{ai}A_{bj}}{A_{aj}A_{bi}}\left(\frac{d_{ai}d_{bj}}{d_{aj}d_{bi}}\right)^{m}\right], \tag{8}$$

whose reciprocal is the inter-station apparent *Q*. Like the TSM, (5) to (8) are all in the frequency domain. The 1/*Q* as a function of the frequency *f* is

$$\frac{1}{Q(f)} = \frac{v}{\pi f\left(d_{aj} - d_{ai} - d_{bj} + d_{bi}\right)} \ln\left[\frac{A_{ai}(f)A_{bj}(f)}{A_{aj}(f)A_{bi}(f)}\left(\frac{d_{ai}d_{bj}}{d_{aj}d_{bi}}\right)^{m}\right]. \tag{9}$$

(9) shows that the RTS does not require any assumptions on the instrument responses and site responses. (9) is similar to (11), but it requires four spectra and four distances, not the two spectra and two distances in the TSM. A pre-determination of *m* is also required, like with the TSM.

Figure 6c shows that the geometry of ideal RTE closely resembles that of RTS except that the positions of stations and events are switched. This case was not presented until the study of Fan and Lay (2003). Similar to (5), we can write

$$\begin{cases} A_{ai}(f, d_{ai}) = S_a(f)R_a(f,\varphi)I_i(f)S_{S_i}(f)G_{ai}(d_{ai})e^{-\frac{\pi f d_{ai}}{v_a Q_a}} \\ A_{aj}(f, d_{aj}) = S_a(f)R_a(f,\varphi)I_j(f)S_{S_j}(f)G_{aj}(d_{aj})e^{-\frac{\pi f d_{aj}}{v_a Q_a}} \\ A_{bi}(f, d_{bi}) = S_b(f)R_b(f,\varphi)I_i(f)S_{S_i}(f)G_{bi}(d_{bi})e^{-\frac{\pi f d_{bi}}{v_b Q_b}} \\ A_{bj}(f, d_{bj}) = S_b(f)R_b(f,\varphi)I_j(f)S_{S_j}(f)G_{bj}(d_{bj})e^{-\frac{\pi f d_{bj}}{v_b Q_b}} \end{cases}. \tag{10}$$

Similar to the RTS, we assume that the velocity structure is one-dimensional and apparent *Q* values are identical at events *a* and *b* in the RTE case, which leads from (10) to (11), the same equation as in the RTS case. The RTM allows the event locations to deviate from the inter-station great circle by two small angles $\delta\theta_a$ and $\delta\theta_b$ in the RTS, and the station locations to deviate from the inter-event great circle by two small angles $\delta\theta_i$ and $\delta\theta_j$ in the RTE. We set maximum values of ±15° (the same as that in the TSM) for those four angles. And the procedure of RTM is also very similar to that of TSM. We follow steps 1) through 5) for each of the four stations, set the same geometrical spreading exponent in 7) as the TSM, and use (9) as the equation to calculate *Q* using a linear regression.

The main disadvantage of RTS is on the typically poor path coverage because of its rigorous geometrical requirement. Thus its feasibility strongly depends on the seismic network. To satisfy the geometry of RTS, continental ray paths of regional distances, inter-station or inter-event distance not less than 150 km, and angle difference within ±15° are required for all the two stations and two events. The RTE provides a dramatic advantage over the rigorous requirements of the RTS. The stations are not required to be deployed in the study area, and can be deployed around a seismic zone within regional distances, which greatly increases the practicability and accuracy of the generalized RTM. Particularly, the RTE can become very efficient in regions with relatively active seismicity and a relatively difficult natural environment for dense seismic networks. The disadvantage is that its resolution is reduced by probable earthquake mis-locations in event catalogs.

The second application of the RTM is that we can use it to solve relative site responses. From equation 10 we obtain

$$\frac{A_{ai}A_{bi}}{A_{aj}A_{bj}} = \left(\frac{I_i}{I_j}\frac{S_{Si}}{S_{Sj}}\right)^2 \left(\frac{G_{ai}G_{bi}}{G_{aj}G_{bj}}\right) \exp\left(\frac{\pi f d_{aj}}{v_j Q_j} - \frac{\pi f d_{ai}}{v_i Q_i} + \frac{\pi f d_{bj}}{v_j Q_j} - \frac{\pi f d_{bi}}{v_i Q_i}\right). \tag{11}$$

Using equation 11 we can solve for the logarithm of the ratio of the site response which gives us a relationship for the relative site response:

$$\begin{aligned} \ln\frac{S_{Si}}{S_{Sj}} = \ln\frac{I_j}{I_i} &+ \frac{d_{aj}-d_{ai}}{d_{aj}+d_{bi}-d_{ai}-d_{bj}} \ln\frac{A_{ai}d_{ai}^m}{A_{aj}d_{aj}^m} \\ &+ \frac{d_{bi}-d_{bj}}{d_{aj}+d_{bi}-d_{ai}-d_{bj}} \ln\frac{A_{bi}d_{bi}^m}{A_{bj}d_{bj}^m} \end{aligned}. \tag{12}$$

And can be further transferred to

$$\begin{aligned} \ln S_{Si} - \ln S_{Sj} = \ln\frac{I_j}{I_i} &+ \frac{d_{aj}-d_{ai}}{d_{aj}+d_{bi}-d_{ai}-d_{bj}} \ln\frac{A_{ai}d_{ai}^m}{A_{aj}d_{aj}^m} \\ &+ \frac{d_{bi}-d_{bj}}{d_{aj}+d_{bi}-d_{ai}-d_{bj}} \ln\frac{A_{bi}d_{bi}^m}{A_{bj}d_{bj}^m} \end{aligned}. \tag{13}$$

Tomographic inversions generally use least squares algorithms such as LSQR (Paige and Saunders, 1982). Constraints on the problem are of great importance and can be introduced using regularization and damping techniques. For example, spatial variations in attenuation are regularized using first or second difference smoothing constraints. Source models, such as MDAC (Walter and Taylor, 2002), can also be included in tomographic inversions for Q. Moments and corner frequencies can be damped to known levels for special events, or regularized to follow a best-fit scaling model (Phillips et al., 2009). Resolution and covariance are quantified using impulse responses, checkerboard tests, and matrix inversion techniques. Such estimates assume that the model equations describe the physics perfectly, which we know is not completely true. Dense networks

such as the Iranian combined networks have allowed us to investigate what are very often unmodeled effects, such as the source radiation, focusing, and medium anisotropy effects mentioned earlier.

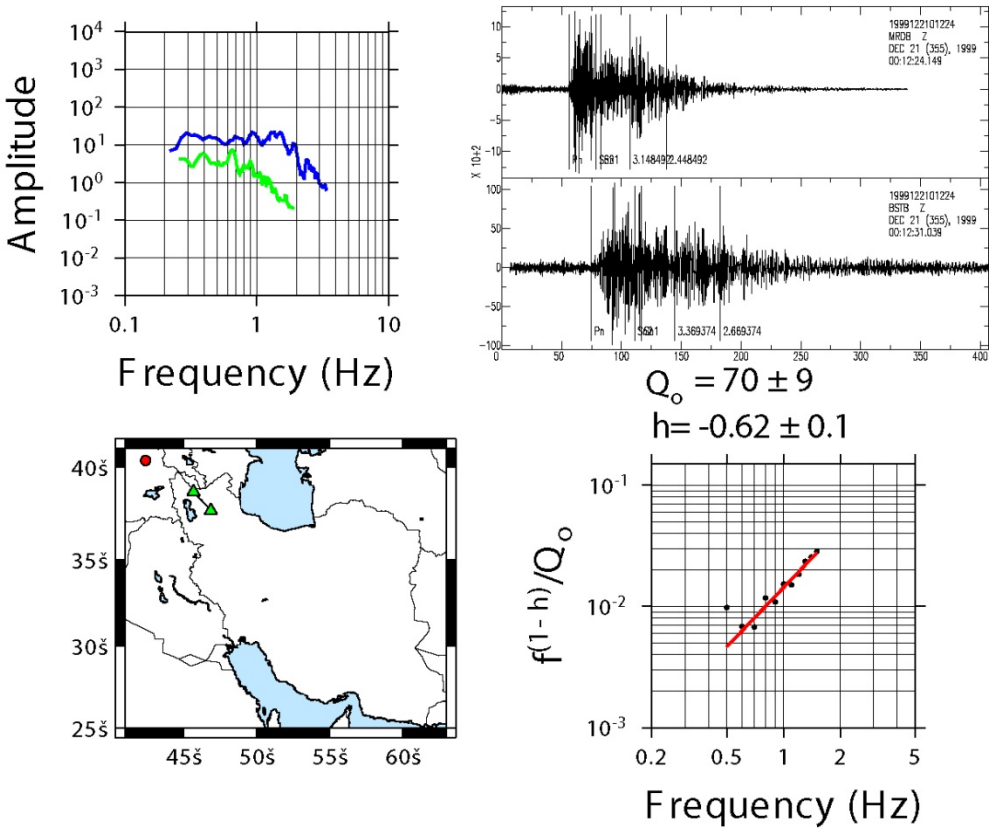

Figure 7. An example of a two station estimate of frequency dependent Q_{Lg} for a two station path in extreme northwestern Iran. This extremely low Q is consistent with other studies in this region.

Attenuation tomography uses estimates of path-averaged attenuation to delineate laterally varying Q. This includes most spectral methods (e.g. Zor et al., 2007). An example of attenuation tomography for Asia using coarsely spaced stations can be found in Xie et al., 2006. Our attenuation (Q) tomography relies on two-station methods for measuring inter-station Q, which cancel the source effect by using station pairs aligned with the source. These methods are relatively straightforward to apply, and are insensitive to source radiation pattern effects, but alignment requirements reduce the amount of data that can be used. We have measured attenuation with the two-station (see Xie and Mitchell, 1990; Xie, 2002; and Zor et al., 2007 for descriptions of the method, including rigorous error analysis) and reversed two station (Chun et al., 1987) methods.

As our derivation of the RTM terms has shown, the reversed method eliminates site as well as source effects. Furthermore we have been able to use the reverse two station approach to isolate the site and calculate the relative site effect. Thus, after correcting for geometrical spreading, we can isolate relative site terms and thereby create maps of relative site terms for the entire Iranian plateau. We can use these relations to determine

both path based Q values that are independent of the site effect as well as a relative site effect term. We have found this to improve attenuation models in particular for Pg attenuation in the Middle East. This has been previously difficult in the Middle East because of a lack of stations and seismic events throughout the region.

Q_0 and η values measured using these methods are of very high quality because they are not subject to the trade-off between source and path parameters, and the smaller data sets can be easily scrubbed with the most rigorous quality control. Measured Q_0 and η values are used to derive a long-wavelength Q map for the Iranian Plateau. This model can be subsequently used as a priori knowledge during amplitude tomography calculations. Alternately, inter-station Q measurements can be included as constraints in the amplitude tomography. Once again, the Iranian combined arrays are ideally designed to tomographically map Q in this region with a high degree of resolution, and have increased resolution in surrounding areas when included in continental scale studies.

3.3 Methodology and Data Summary

We have used high-quality regional waveforms recorded at 589 broad-band and short-period stations operated permanently or temporarily over the Iranian and Turkish plateaus, and along the Dead Sea fault region. We employ stations from different networks operated by different institutions and the data have been collected from a wide variety of recording systems. We have therefore paid very careful attention to the instrument responses of the stations and verified the responses using the spectra of the background noise and/or large magnitude teleseismic seismograms and calibrated the instrument responses if marked differences were observed between a given station and adjacent stations. We noticed that at some stations, the static gain needed to be calibrated. Because of similar dispersion behavior of higher modes of Rayleigh and Love waves at Lg frequencies, Lg waves exhibit roughly similar characteristics on three components of seismograms (Campillo, 1990). We therefore computed Lg spectra from the vertical component seismograms because of the higher signal-to-noise ratio on this component at most stations. The Lg window is manually picked on each vertical seismogram with a fixed group velocity window length of 0.7 km/s while the upper limit of the Lg group velocity is allowed to vary between 3.8 km/s and 3.3 km/s. We have analyzed data from 589 stations and 28795 Lg spectra have been collected from 2990 regional earthquakes with a magnitude of 4.0 or higher. Reliable measurements of crustal attenuation using Lg waves are difficult to obtain because the Lg wave amplitude at a station depends upon many factors including source spectra, radiation patterns, 3D velocity structure along the travel paths, local site effects at stations, and instrument responses of the recording systems. To eliminate the effects of source spectra and 3D velocity structure on Lg Q estimates, we use the Two-Station Method (TSM) introduced by Xie and Mitchell, (1990). This method requires strict recording geometry and hence dense station and event distribution. Non-identical site conditions and likely erroneous instrument responses can affect the TSM Lg Q measurements. The reverse two-station/event method (RTM) (Chun et al., 1987) can be employed to further eliminate the effect of site and instrument response on Q measurements. This method however requires more severe recording geometry, which in turn dramatically diminishes the ray coverage. On the other hand,

very dense ray coverage is required to explore the lateral variations of the Lg Q. We first used the TSM Lg Q measurements for the regionalization of crustal Lg Q and subsequently compared the Lg Q model obtained from the TSM measurements to that obtained from RTM measurements. We present here the TSM and RTM Lg Q measurements centered at 1 Hz (Q_0) and their frequency dependence factor (η). In order to reduce the error in our measurements and satisfy the assumptions made by the TSM method (Xie and Mitchell, 1990; Xie et al., 2004), we choose station pairs at least 150 km apart and aligned within 15° (an example is shown in Figure 7). In order to further refine the measurements, we select those measurements with low estimated errors in both Q_0 and η. More than 6900 individual TSM Q_0 measurements from 2405 TSM ray paths satisfied these criteria with repeated measurements along some paths. The repeated measurements at a given path are averaged. The selected TSM Q_0 measurements include 600 measurements from blocked paths in order to improve the ray coverage. These measurements come from the database of blocked paths from our review of all regional phase waveforms in our database (see Figure 5). We include these blocked paths by estimating a maximum Q needed to block Lg for the given event-station distance. This will potentially bias our Q model towards higher Q values, however, we have found that our model is not greatly affected by including these paths.

One problem with our models is that to determine a Q value we must have an observable Lg phase, however, for many longer paths across the northern Middle East Lg is blocked therefore there is no amplitude that one can use to calculate a Q value. This absence of data can also serve to bias our Q models upward by not including these blocked path, however, including these paths can always introduce significant noise since we are not really able to measure the true attenuation only place an upper limit or constraint on the Q. In order to minimiz the noise into our model and to include the most important blocked paths (i.e. those that occur over a relative short distance) we chose only those measurements from blocked paths that yield Lg Q_0 not in excess of 250. This in effect applies a maximum blocked path length that we include in our model. For a Q of 250, the maximum distance is approximately 700 km depending upon what you assume our signal to noise value is for each blocked path ($R_{max}=\ln(SNR)*Q_{min}v/\pi f$). We apply this threshold to avoid possibly overestimating Q_0 values from very long blocked path. Even if these longer blocked paths would produce reliable minimum Q values, they would add little to the Q model since the paths are very long. Figure 8 shows the 2405 two-station paths with colors indicating the averaged Q_0 over each path. The averaged TSM Q_0 and η values are subsequently inverted using an LSQR algorithm to map the lateral variations of Lg Q_0 and η over the regions covered by the TSM ray paths. To parameterize the tomographic model, the study area is divided into 0.75°-by-0.75° cells.

4. RESULTS AND DISCUSSION

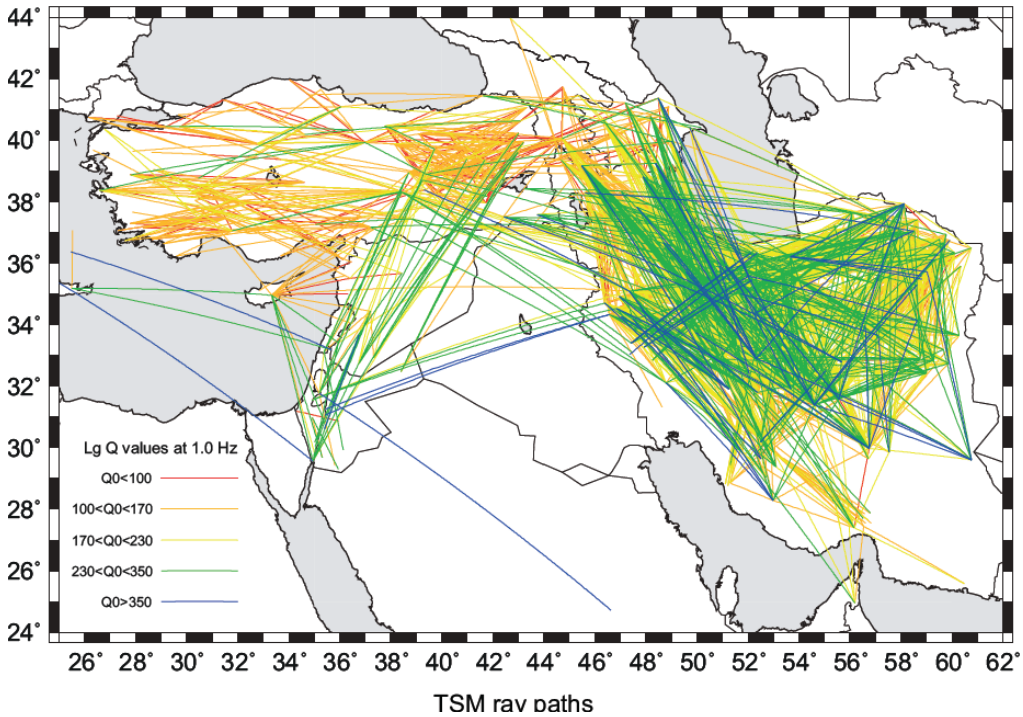

Figure 8. Map showing the Two-station (TSM) ray paths color-coded according to their respective Lg Q_0 (at 1 Hz) values.

4.1 Lg Q Tomography: Two Station Results

The Q models obtained using the TSM and RTM methods are generally in agreement in in terms of relative Q variations,; however, we do observe consistent differences in terms of absolute Q. Q values in the TSM map are probably contaminated with the local site effects and possibly incorrect instrument response functions. Lg Q values of around 200 are mapped over most parts of central Iran and less than 150 over the Anatolian Plateau. Patches of Lg Q >> 300 are observed in the Zagros, central Alborz Mountains, Iranian Lut block, western margin of the Caucasus Mountains, and north of the Dead Sea region. Low Lg Q (<100) are mapped in eastern Turkey and NW Iran. Better ray coverage is obtained with the Two-Station method (TSM) than the Reverse Two-Station method (RTM). We observe higher Q paths over the Iranian Plateau compared with those over the Turkish Plateau.

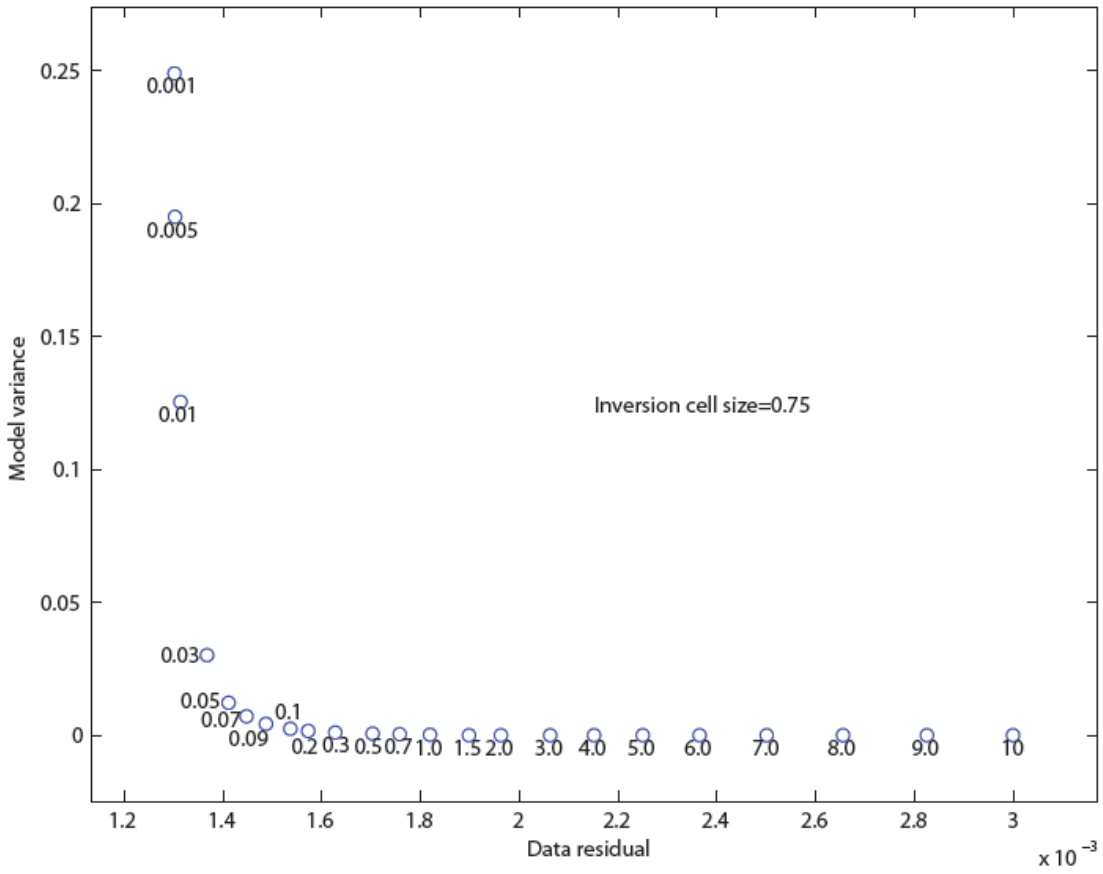

Figure 9. Data residual versus model size for our Lg tomography at 1 Hz (Figure 10). The damping parameters are shown below each of the blue dots. We have chosen 0.1 for our damping factor.

We have experimented with large numbers of different damping parameters and cell sizes to test whether these very abrupt anomalies are implied by the data or not. We selected the damping factor using the traditional plot of residual (error) as a function of damping:

We made L-curves from multiple iterations of our tomographic inversions to determine which damping factor is suitable for each inversion. The L curves of the inversion suggest that we use different damping when using the unblocked Lg Qs with an inversion cell size of 1 deg by 1 deg and 0.5 deg by 0.5 deg. The value of the damping factor is indicated by the inflection point along the L-curve. From these L-curves, we believe that a damping of 0.1 or 0.05 is the best one for these inversion cell sizes. It may be that Lg Q in the Middle East changes very abruptly even within the same tectonic terrane. This has important implications for using larger scale smooth models to predict amplitudes at closer distances.

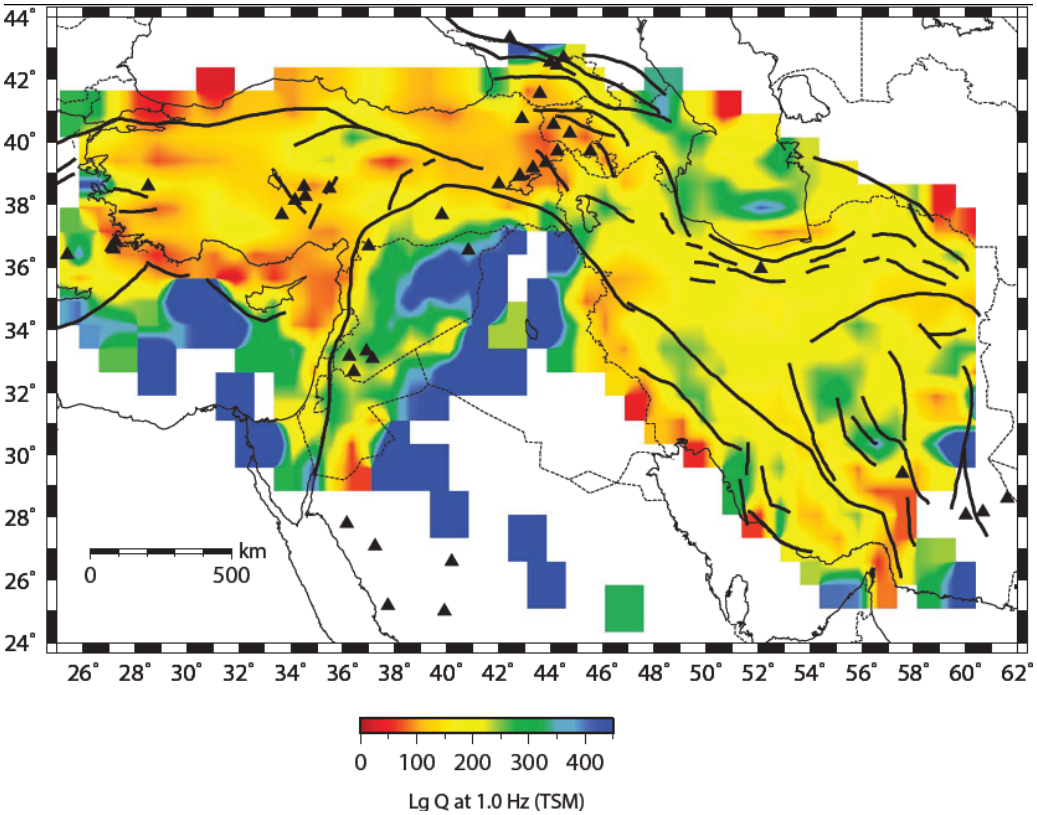

Figure 10. Two-station (TSM) Lg Q_0 tomographic map as obtained by including blocked paths. Thick black solid lines depict the major faults and black triangles indicate the location of the quaternary volcanoes. For reference to tectonic setting refer to Figure 2.

Figure 10 shows the tomographic regionalization map of the TSM Lg Q_0. In Figure 11 we show the TSM Lg Q_0 tomographic map obtained only using unblocked paths. The most prominent feature in the TSM Lg Q_0 map (Figure 10) is the difference between the Turkish-Anatolian and Iranian plateaus. The Turkish-Anatolian plateau is mostly characterized by Lg Q_0 lower than 150 whereas the Iranian plateau exhibits significantly higher values ranging between 200 and 300. The south Caspian basin does not show very low Q values; on the contrary we observe some high Q values in the northern and western parts of the S. Caspian basin. Although the ray coverage is not adequate for well resolved lateral variations in the S. Caspian, examination of individual RTM and TSM measurements confirms the presence of high Q values along these paths across the S. Caspian even though we have observed many paths with blocked Lg across

the S. Caspian. It is possible that for the Lg phases that appear to cross the S. Caspian that the Lg energy is either travelling below or more likely around the oceanic crust. It is more likely that the Lg energy is bending around the basin because the basement part of the crust is likely less than 10 km thick. The Lg Q_0 along the Zagros belt shows some variations with values ranging from lower than 100 to ~300. Some areas with relatively higher values of Lg Q_0 are observed in the Lut Block in central Iran. The highest Lg Q_0 values are mapped over the Arabian platform in northern Iraq separated from the low Q region of the Turkish Plateau by the Bitlis suture zone.

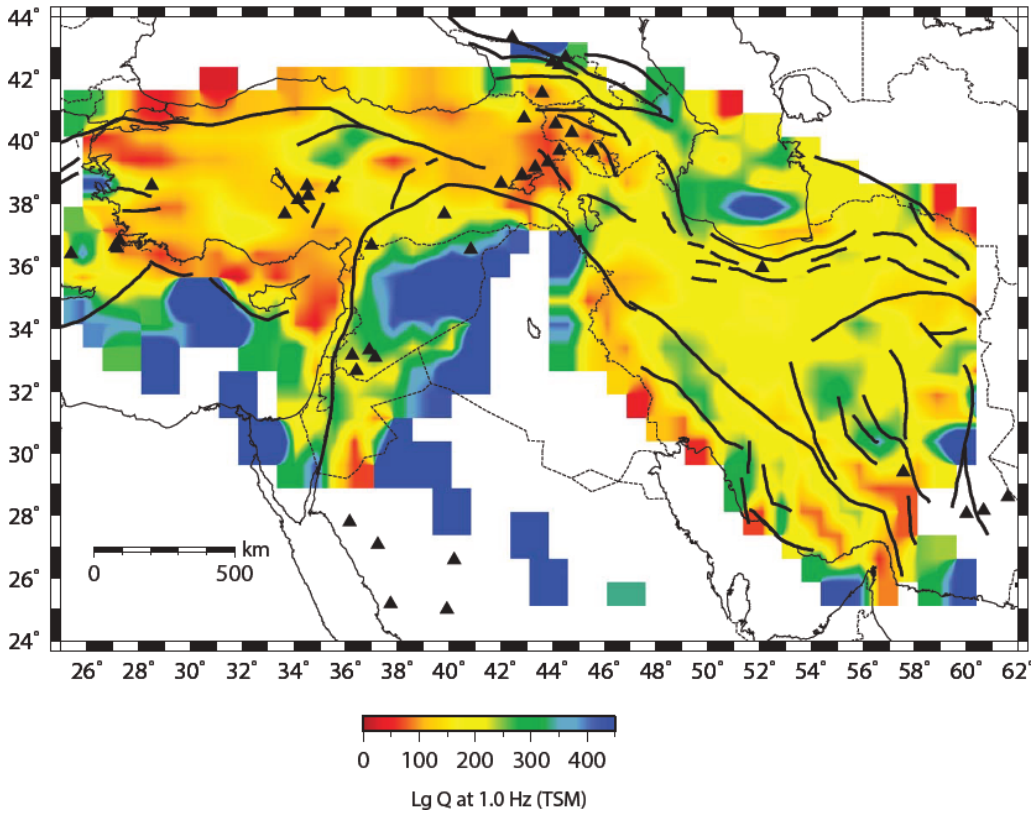

Figure 11. Final two-station (TSM) Lg Q_0 tomographic map as obtained without blocked paths. Thick black solid lines depict the major faults and black triangles indicate the location of the quaternary volcanoes. For reference to tectonic setting refer to Figure 2.

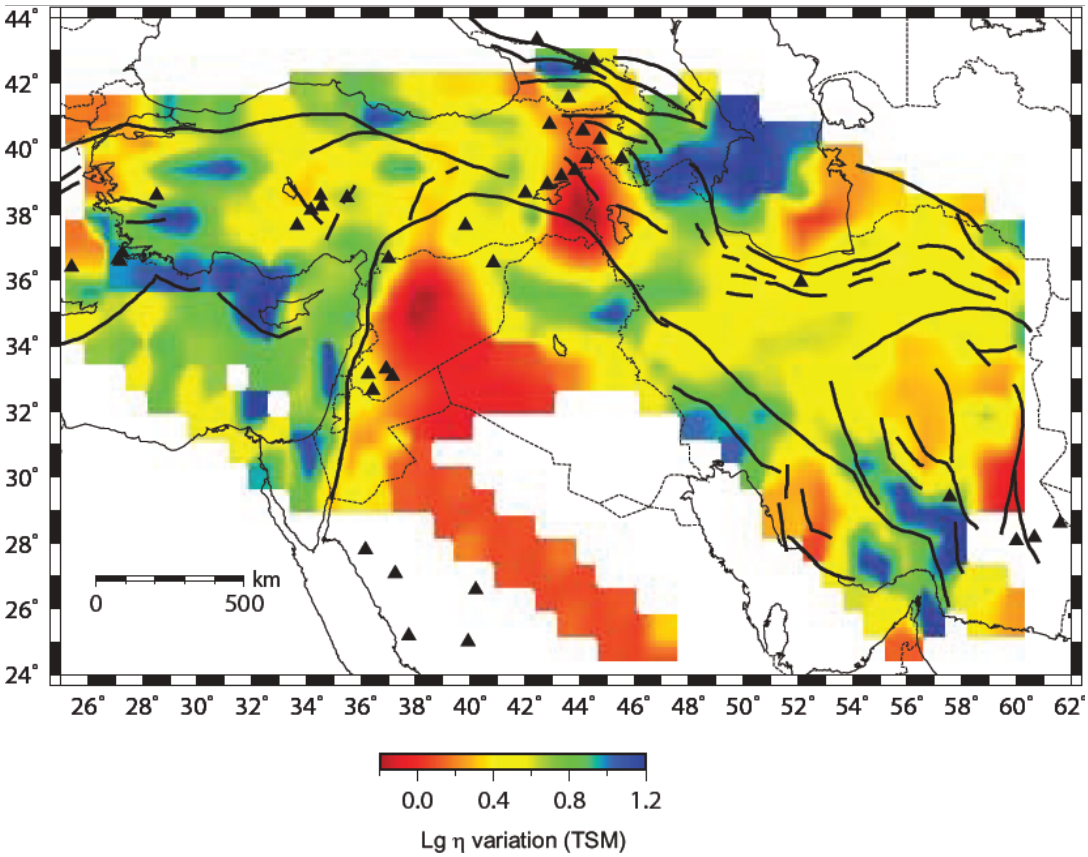

Figure 12. Final two-station (TSM) Lg Q_0 frequency dependence map as obtained without blocked paths. We obtained the frequency dependence by making Q measurements over a wide range of Lg frequencies.

4.2 Lg Q Tomography: Reverse Two Station Results

As discussed above, the TSM Q measurements may be contaminated by relative differences in the local site effects and improper instrument response corrections. The RTM approach avoids these errors; however, it dramatically reduces the ray coverage. We utilize the RTM measurements as a touchstone to verify the accuracy of the TSM measurements. We selected those RTM measurements that passed through the screening criteria as stated above for the TSM measurements. We selected 9551 RTM measures over 793 RTM paths and averaged the repeated measurements. The RTM ray coverage is reasonably dense in central Iran and Eastern Turkey, it is very sparse in NW Iran, S. Caspian, western Turkey and the central Anatolian plateau. We inverted the averaged RTM Lg Q_0 in the same manner as the TSM Lg Q_0 in order to compare the Lg Q_0 maps obtained using the two approaches. The RTM Lg Q_0 map in Figure 4 shows features very similar to those observed on the TSM Lg Q_0 map in Figure 3. To examine the resolution, we performed two-dimensional checkerboard tests using the TSM and RTM ray geometries as used to produce the Lg Q_0 maps. The checkerboard test results for both the TSM and RTM Lg Q_0 tomography are shown in Figure 14. The checkerboard tests illustrate that Lg Q_0 anomalies with a size of 1.5°-by-1.5° can be well resolved by our TSM ray coverage over the Anatolian, Turkish and Iranian plateaus. The anomalies cannot, however, be well retrieved in the Arabian plate, the Mediterranean, the S. Caspian, or on the margins of the models. The Lg Q_0 anomalies appear to be smeared

along the Zagros belt as well. The RTM checkerboard test reveals that with the present RTM ray coverage the Lg Q_0 anomalies may be well resolved in central Iran and Eastern Turkey. In other regions, the RTM Lg Q_0 tomography model has very poor resolution.

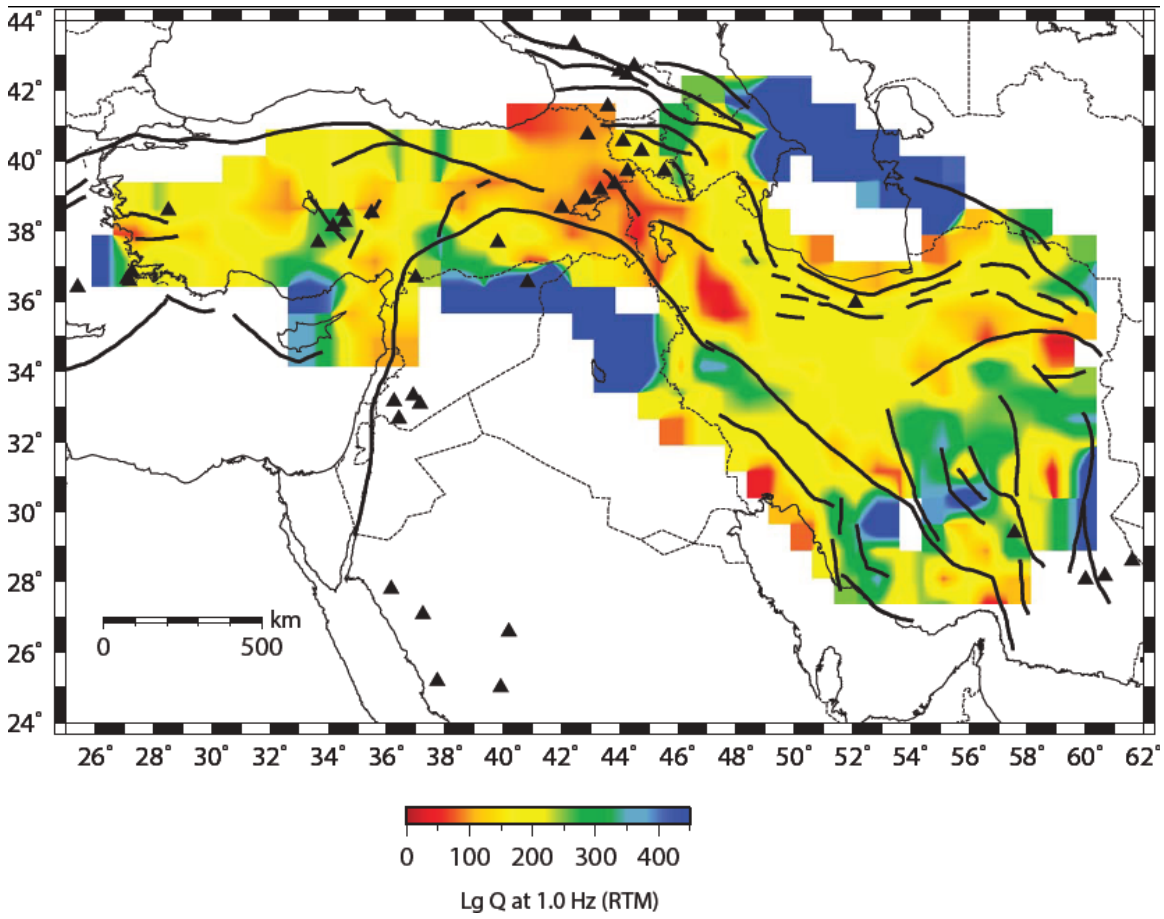

Figure 13. Our final reverse two-station/event (RTM) Lg Q_0 tomographic map. The description of the tectonic features is as stated in Figures 2 and 3.

In addition to the Lg Q_0 value, we have used the TSM and RTM methods to determine the frequency dependence of Q assuming the power law relationship: $Q(f)=Q_0 f^{\eta}$. The frequency dependence of Q provides clues to the mechanism of attenuation. Weaker frequency dependence typically suggests an intrinsic attenuation mechanism whereas a strong frequency dependence implies that scattering attenuation is the dominant mechanism for the observed attenuation (e.g. Dainty, 1981; Bao et al., 2012). In the TSM and RTM methods, η is estimated by the slope of the linear function fitted to the Lg spectral ratios between two stations in function of frequency (Figure 15). Therefore, measuring η requires calculation of spectral ratios between two stations at a sufficiently wide range of frequencies around the reference frequency (1 Hz) and therefore exhibits consistently larger errors. We therefore apply stricter screening criteria to the selection of η and choose only those η measurements that show very low error in both η and Lg Q_0.

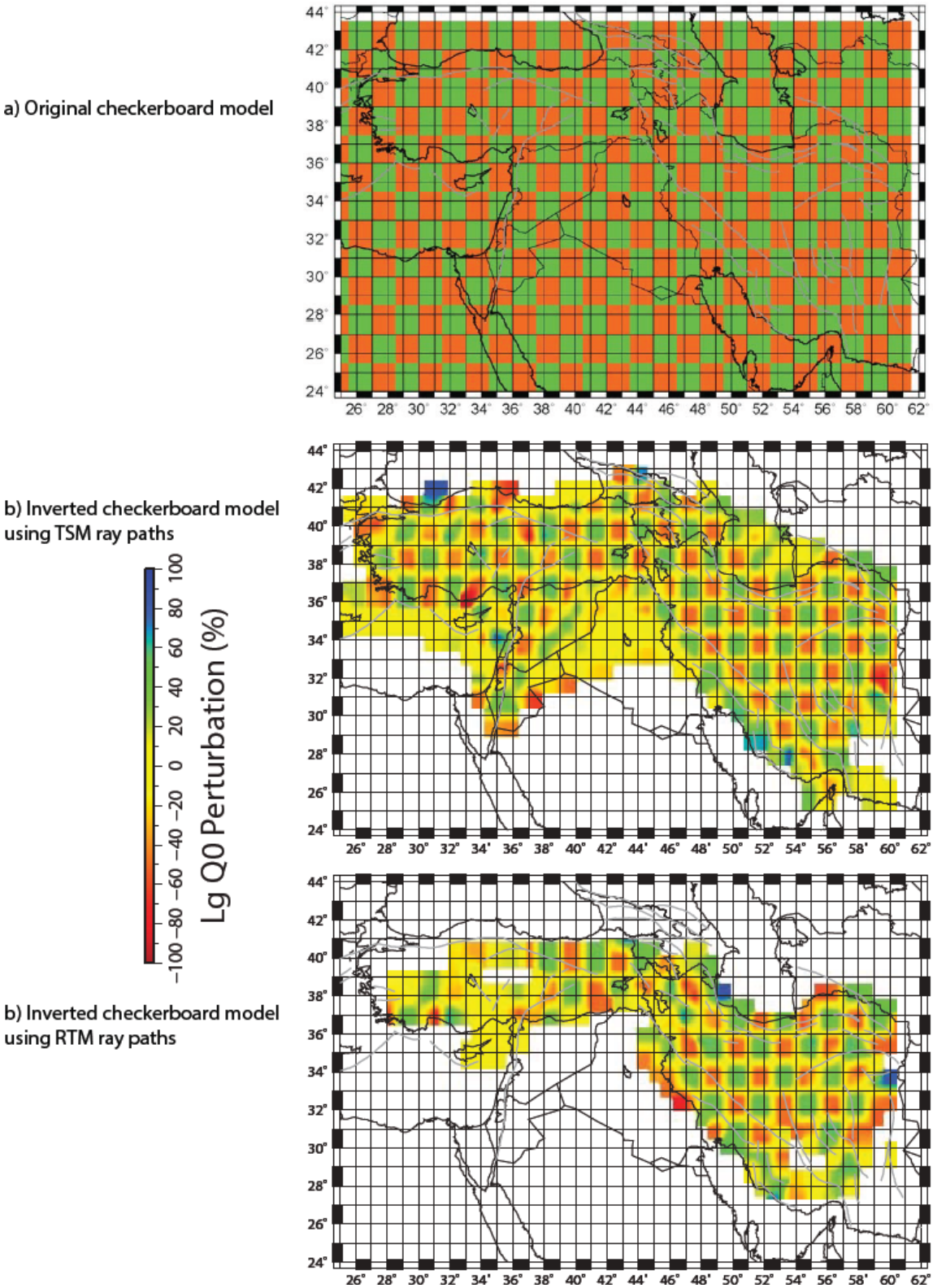

Figure 14. Checkerboard tests for both the (b) TSM tomographic model and the (c) RTM method. We have introduced 10% gaussian noise for this particular resolution test. This might be a bit low for Q measurements. The anomalies have a size of 1.5 degrees by 1.5 degrees.

This subsequently reduces the number of η measurements relative to the Lg Q_0 measurements. We use the same LSQR algorithm as used for Q_0 to map the lateral variations in η. The TSM and RTM η maps are shown respectively in Figure 12 and 15. The η maps obtained from the two approaches exhibit very similar characteristics. For the most part, η ranges between 0.4 and 0.8. In the northern part of the Arabian plate, we observe very low η values in a region with relatively high Q_0 values (Figure 13). There are other low η regions in the eastern Turkey and NW Iran where the Q_0 values are also low. The observation of both low Q_0 and low η can be explained by high intrinsic attenuation due to the presence of fluids, partial melt, and high temperatures in the crustal rocks (e.g., Mayeda et al., 1992*;* Mitchell, 1997). We observe a region of relatively high frequency dependence in the western S. Caspian and eastern Caucasus. This region is characterized by relatively high Lg Q_0 values. The high frequency-dependence and high Q_0 values may be because of some focusing effects due to lateral velocity changes that could not be accounted for by a 1-D geometrical spreading assumption.

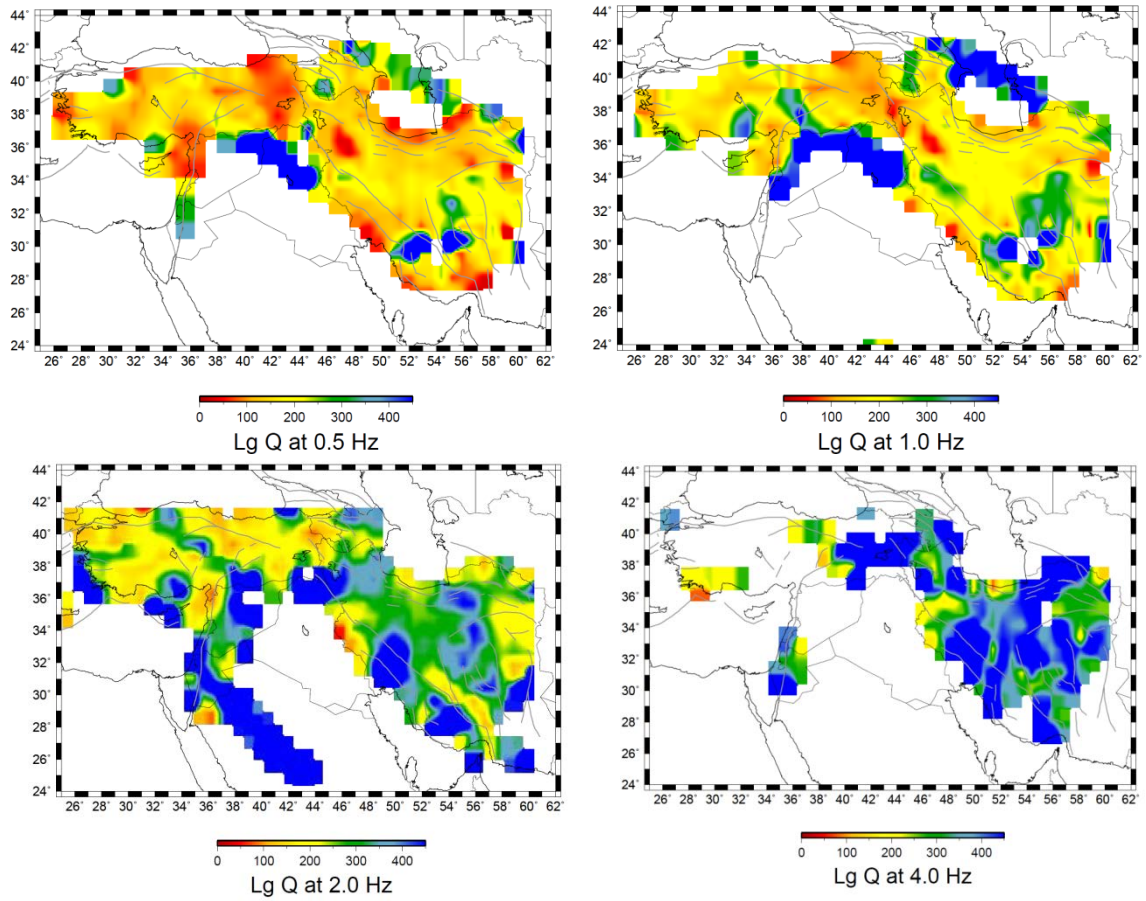

Figure 15. Frequency dependence of our RTM Q values across the northern Middle East. It is important to note that we have very limited data and signal to noise may be quite low.

During the process of picking the Lg window on individual seismograms, we have also noticed that the Lg group velocity systematically varies for different regions. We were able to map the variation of the Lg group velocity variations by inverting the Lg arrival time picked on individual seismograms. We use the LSQR algorithm modified for velocity inversion to invert the Lg arrival time residuals for Lg group velocity

perturbations. The travel time residuals are calculated relative to arrival time for a laterally uniform group velocity of 3.5 km/s and the perturbations are thus relative to this velocity. The resulting group velocity perturbation maps are shown in Figure 17. It illustrates that, in general, the central Iranian blocks are characterized by higher Lg group velocities relative to the Anatolian and Eastern Turkish Plateaus. This result is in agreement with the Lg Q_0 maps (Figures 10,11, and 13) assuming the low Q should correlate with a low Lg group velocity. The highest Lg group velocity is observed across the S. Caspian block likely due to the travel paths through the high velocity oceanic type basement rocks. The lowest values are found for the Mesopotamian Foredeep (Figure 17 and 2) that can be attributed to the deep young sediments deposited in this foreland basin.

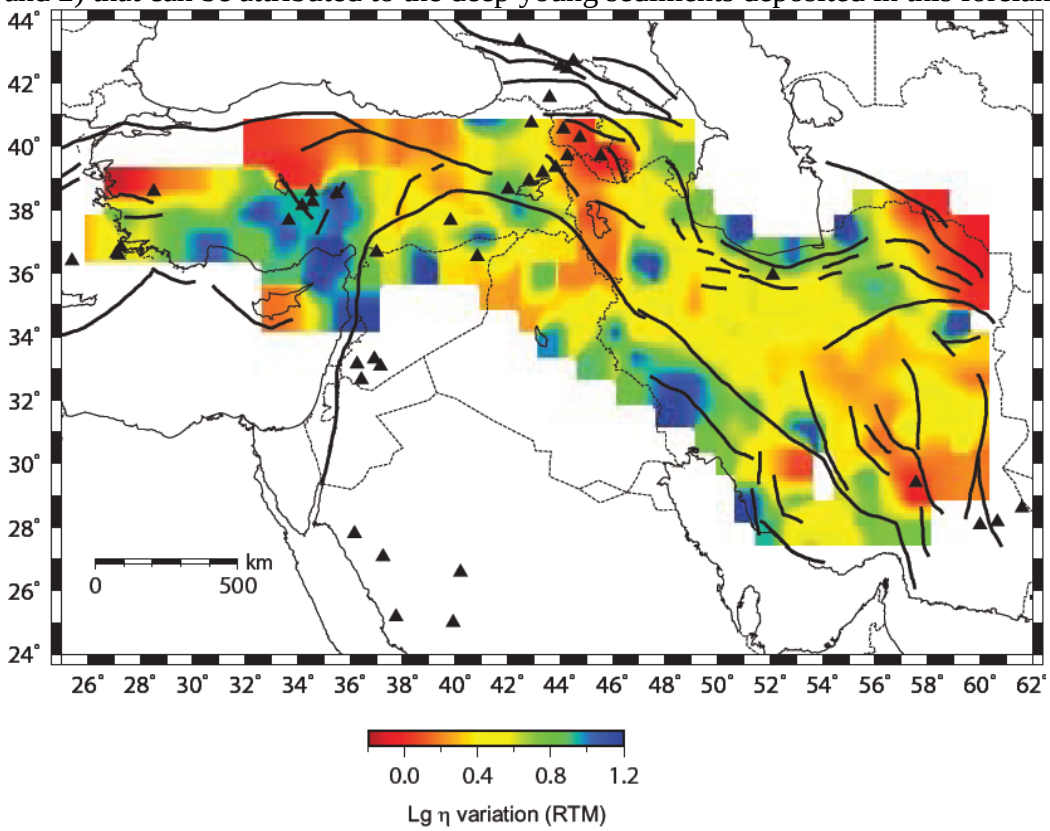

Figure 16. A plot of the frequency dependence for our RTM Q model. This is another way to view the frequency dependence of our RTM Q measurements as compared with Figure 15. We observe some difference with the TSM frequency dependence as seen in Figure 12. This might indicate that site excitations might be more greatly affecting the frequency dependence of Lg Q.

In an attempt to quantitatively show the correlation between the Lg Q_0 and Lg group velocity maps (Figure 10,11, and 13), we calculate the value 1-abs(normalized Lg group velocity-normalized Lg Q_0) as a measure of correlation in each cell of the map and then plotted the correlation values (varying between -1 and 1) in Figure 18. To normalize our models we first divide both the Q and group velocity models by their respective mean values (200 for Lg Q and 3.5 km/s for the group velocity). We then normalize these Q and velocity perturbations to 1 by dividing by the maximum perturbation (approximately 300 percent for Q and 0.4% for the velocity) This figure shows that the Lg Q_0 and Lg group velocities are very well correlated over most of the region. There are two regions with a negative correlation between Lg Q_0 and group velocities. The first region is the

northern margin of the Arabian plate south of the Bitlis Suture where high Lg Q_0 and moderate to low Lg velocities are observed; the other region is the northern Mediterranean Sea that is characterized by low Q_0 values and high Lg velocities.

Our crustal Lg group velocity model (V_{Lg}) in Iran is comparable to the velocity models given by Mottaghi et al., (2013) from tomographic inversion of short-period group and phase velocity dispersion data of fundamental-mode surface waves obtained by analysis of ambient-noise records at broad-band stations. Their models, though frequency dependent, show most of the main features in our average crustal Lg wave group velocity model. These main features are the low velocity regions in NW Iran, relatively low velocity crust beneath the Zagros and Alborz, and relatively high velocity crust along the MZRF and beneath Central Iranian blocks. This example shows that Lg travel times, when precisely picked, can serve as a reliable proxy to estimate average crustal shear wave velocity. In this regard, our crustal V_{Lg} model presents the first comprehensive crustal seismic shear-wave velocity model covering the entire region of the Northern Middle East.

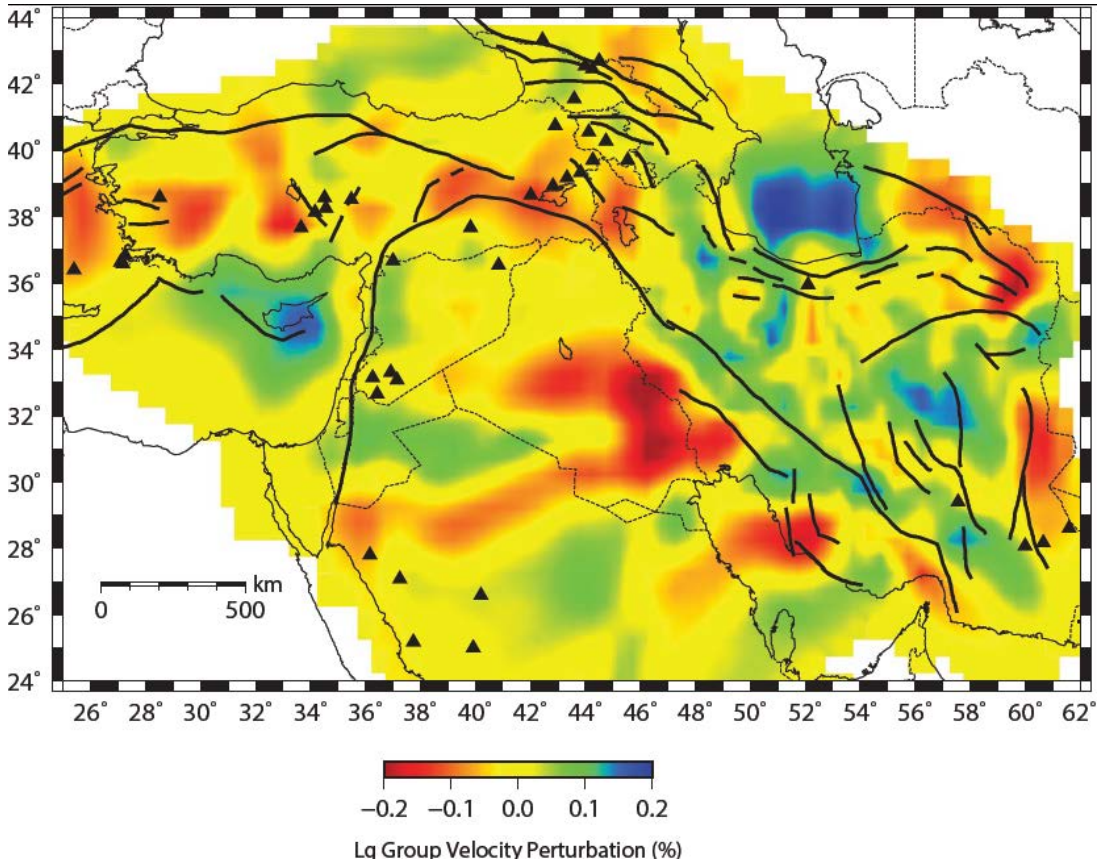

Figure 17. Our map of Lg group velocity variation across the Middle East. This is in effect the variation in peak group velocity. The average peak group velocity here is 3.5 km/s.

A comparison of Figures 17 and 18 may suggest a likely mechanism for the attenuation of high freqeuency shear waves across the Middle East. This postive correlation is suggestive that hotter crustal rocks possibly combined with crustal melt (in eastern Anatolian and the Menderes massif in western Turkey) is primarily responsible for Lg

blockage and the regions with very low Q values. In contrast, we observe poor correlation in the northernmost Arabian plate where it is likely that thick sedimentary sequences significantly lower Lg group velocities but do not appear to have as big of impact on crustal shear wave attenuation (Lg Q). Of course these regions are currently at the edge of our Lg Q model and more stations within the Arabian plate will help to confirm verify this hypothesis.

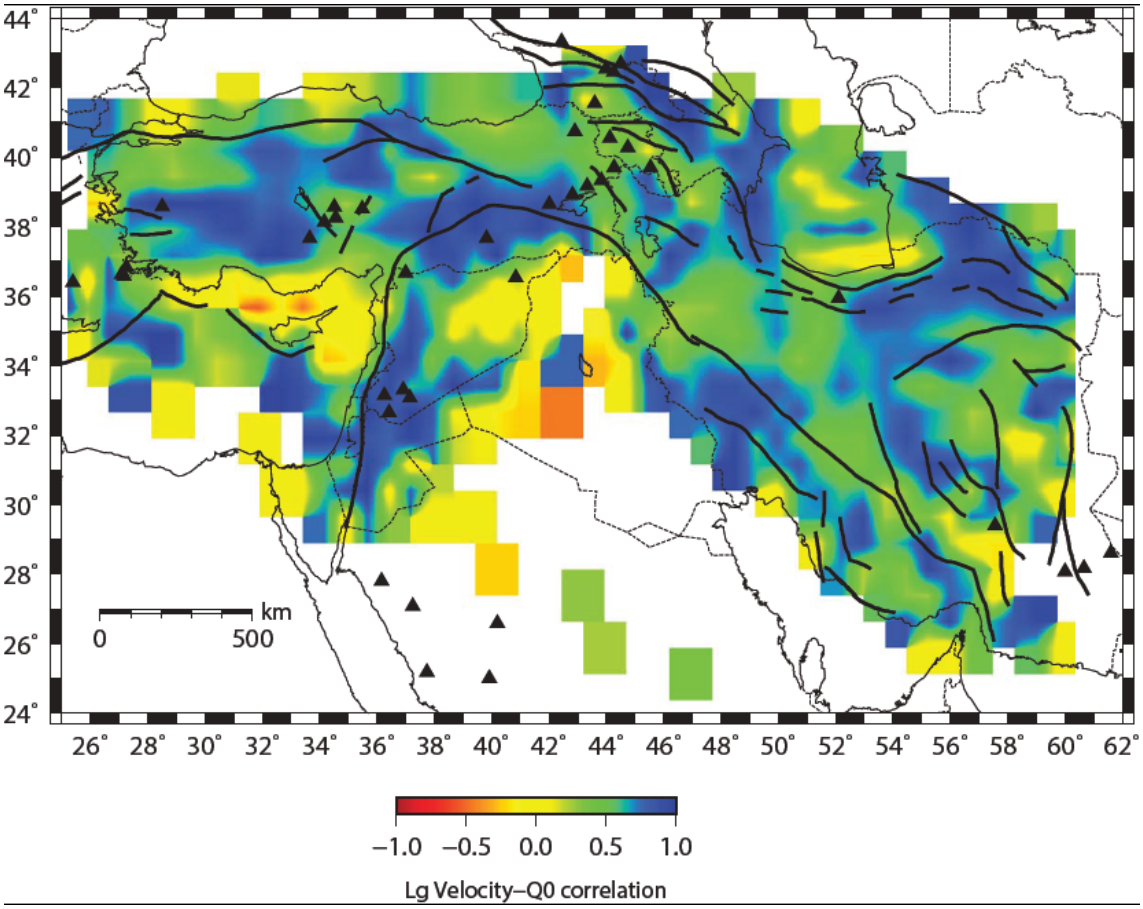

Figure 18. The correlation between our Lg group velocity (Figure 17) and our TSM Lg Q tomographic model (Figure 12). We see a positive correlation between most of the model with the exception of regions with thick sediments where there is likely a strong compositional influence on the Lg group velocities.

4.3 Lg Q Tomography: Reverse Two Station Site Terms

We have also constructed a model of absolute site excitation using the Reverse Two station Method (RTM). Firstly, however we attempted to test and improve upon the instrument response data we had for stations in the Middle East. We spent approximately six months carefully comparing the background noise levels for all stations as well as the long period signal from teleseismic surface waves. Using the RTM method and the formulation shown in equations 12 and 13 we can test the reliability of our instrument response estimates by calculating the relative site terms. Using this method we found and corrected many inconsistencies between the IRIS and KOERI instrument response. The site terms calculated from the improved instrument responses can be seen in Figure 19

where our RTM site terms have been reduced a great deal compared to our initial models, suggesting that we have likely improved upon the original instrument response data. We still have a few problem stations in western Turkey and eastern Iran where it appears the gains might not have been reportedly accurately. We have also looked at the frequency dependence of the site terms to see if whether the remaining signal is consistent with the gain still begin wrong or due to local site amplification. In general the frequency dependence is relatively weak again suggesting that we have most likely improved upon the instrument gain data we original obtained from network operators.

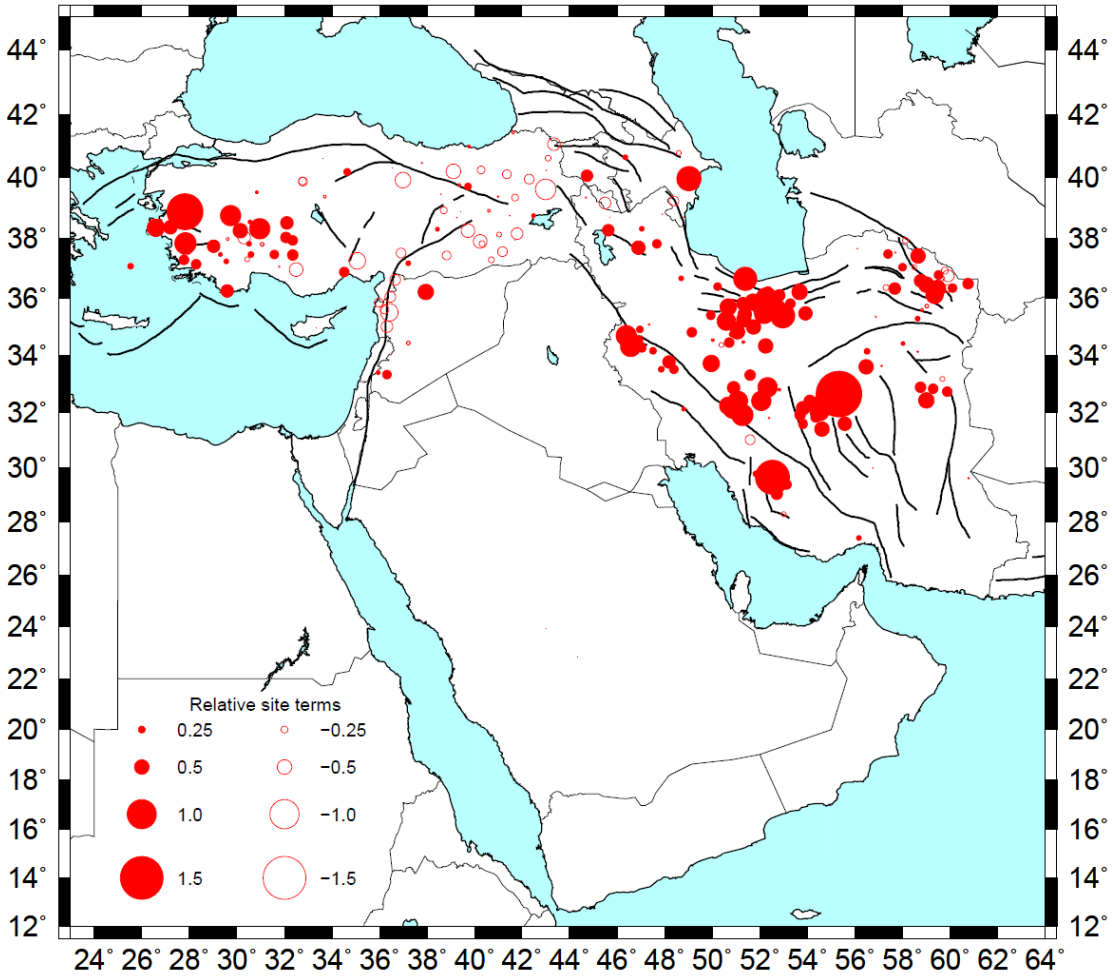

Figure 19. A plot of the logarithm of the absolute site terms estimated from our individual relative site terms taken from equation 11. These absolute site amplification values are relative to the entire network average.

The frequency dependence of the site terms is shown in Figure 20. In general we observe positive site amplification in regions with thicker sediments such as the Menderes Massif rift basin in western Turkey and the Lut block which has relatively thick sediments underlain by a stable continental crust that has likely not experienced as much internal deformation as other parts of the Iranian plateau. In eastern Turkey we observe a de-amplification of the signal that is somewhat similar to what we observed in the high elevations regions of Tibet. The other

similarity is that eastern Turkey is a crustal mélange with very few sediments and have been recently uplift.

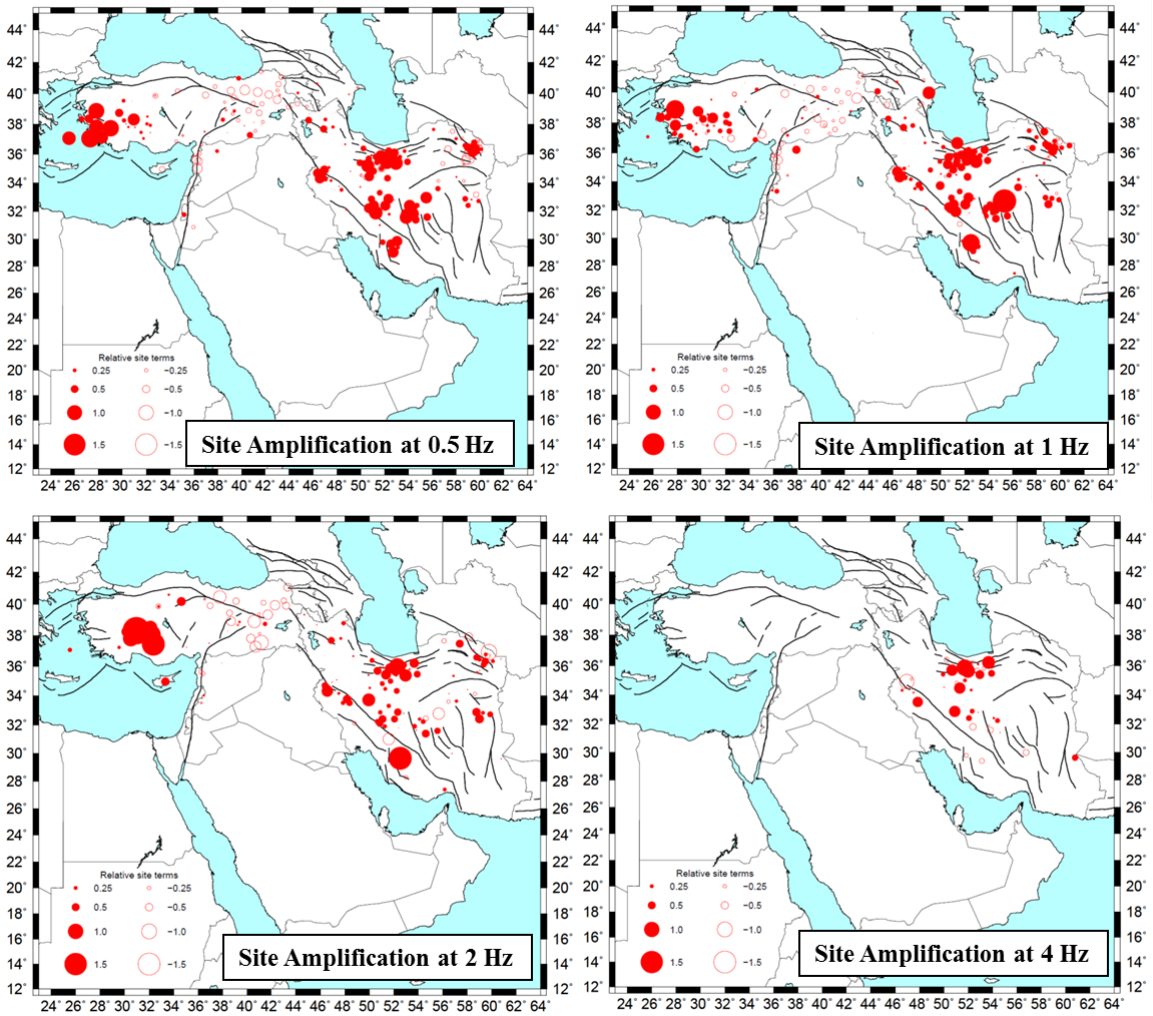

Figure 20. A plot of the frequency dependence of the absolute site terms with respect to the Middle Eastern Network average at 0.5, 1, 2, and 4 Hz. The 1 Hz model is the same as Figure 19. Once again the site terms for our 4 Hz data are somewhat questionable due to possible issues with signal to noise at high frequencies. This is also the reason for the relative low number of station terms at 4 Hz.

At 4 Hz we see some evidence of frequency dependence for the few stations that we have reasonable signal to noise at that high frequency. The stations in the Alborz Mountains, however, do not change appreciably even that 4 Hz. Some stations in the central Zagros, however, show some evidence of frequency dependence. These stations are temporary, however, so the response might not be as reliable as the permanent stations.

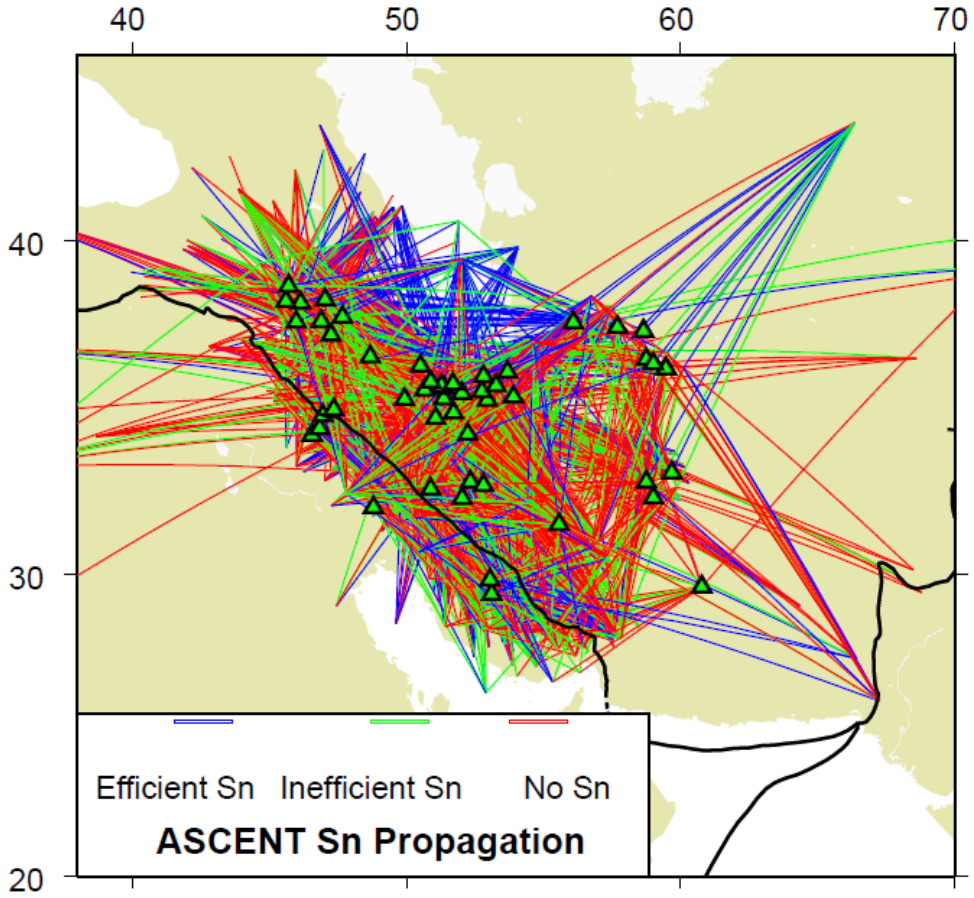

Figure 21. An efficiency map for long period Sn where we define long period as between the frequencies 0.5 and 0.1 Hz. Note that we find very few efficient and inefficient paths except for paths that cross the south Caspian Sea. This database is taken from four years of data from the combined networks shown in our quarterly reports.

4.4 Sn Q Tomography

It is well known that Sn propagates weakly or not at all beneath the Iranian plateau, but propagates efficiently beneath the south Caspian sea and Arabian plate (Sandvol et al., 2001). We began this project working on long period Sn; however, we found that long period Sn was also often blocked across the Iranian plateau.

We used a large waveform data set including 92 stations and 31 events from 1996-2011, the two-station path coverage is shown in Figures 21 and 22.We used a bandpass filter (0.1-0.5 Hz) to identify efficient long period Sn phases. As with Lg, we manually picked and visually inspected all Sn waveforms, eliminating all blocked Sn paths shown in Figure 21. We inspect both long period (~0.3 Hz) and high frequency bands. We found that we typically observe Sn at longer periods for earthquake magnitudes larger than 4.5, so we eliminated any smaller events. This limitation is offset by the fact that we have over twelve years of data from various Iranian networks used in our Lg Q work. The data were sufficient to compile 3200 two station paths; however, our azimuthal coverage was not optimal.

In order to determine Sn Q we applied a Two Station Method (TSM) to eliminate the source effects. We used the LSQR algorithm to tomographically map Sn Q values across the Iranian plateau (Figure 24). We investigated the frequency dependence of the Sn Q values by defining several different narrow band and solving for the Q value at the center frequencies. We used three different frequency bands: 0.1 - 0.5 Hz, 0.5 - 1.5 Hz, and 1-3 Hz.

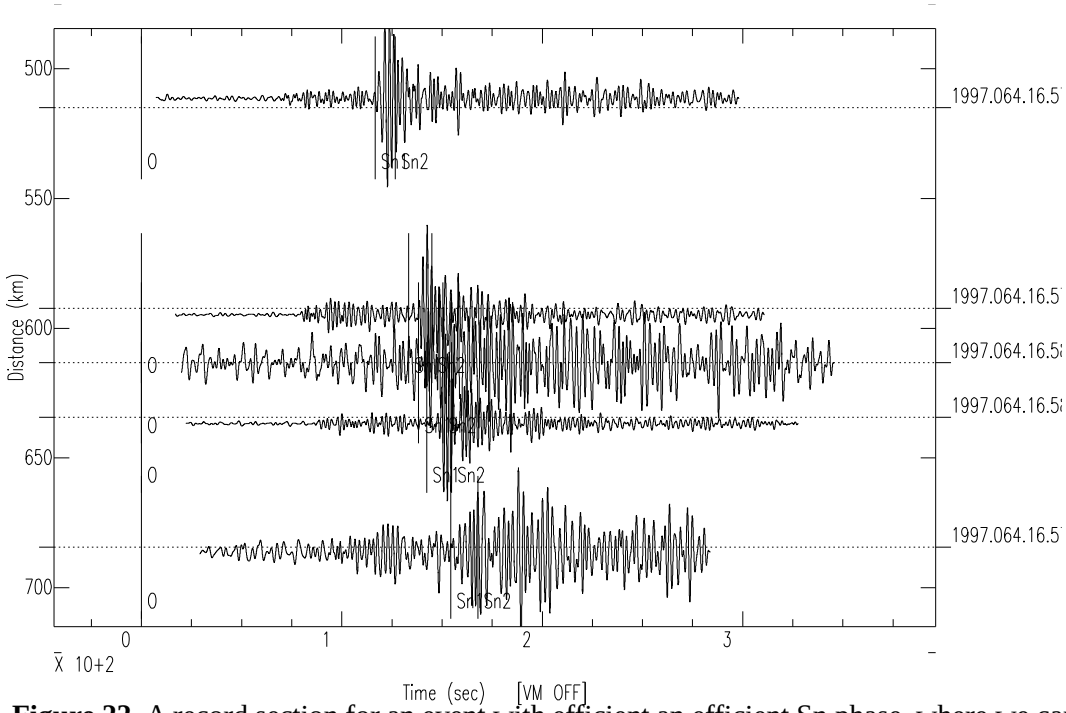

Figure 22. A record section for an event with efficient an efficient Sn phase, where we can begin to see strong attenuation past 700 km distance.

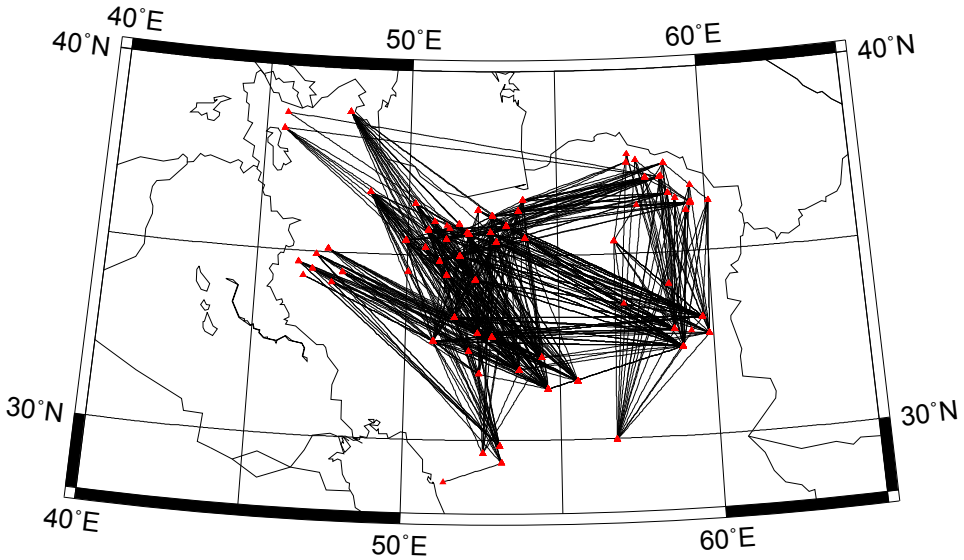

Figure 23. A map of 3162 two-station paths for Sn Q values calculated by 31 big events from 1996-2011 using 427 waveforms with 92 stations.

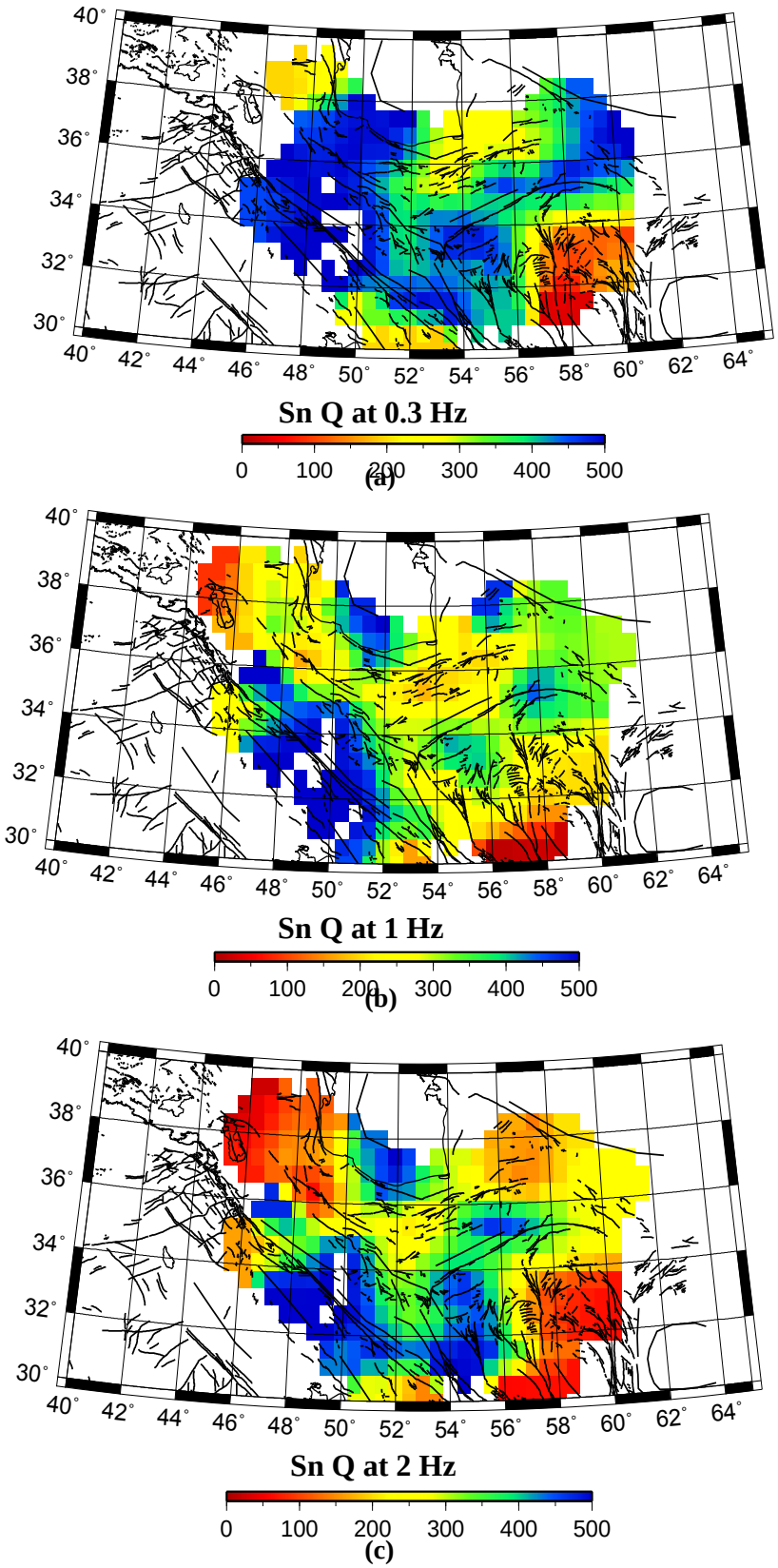

Figure 24. (a) Sn attenuation tomography at 0.3 Hz; (b) Sn attenuation tomography at 1 Hz; (c) Sn attenuation tomography at 2 Hz.

Our preliminary results show somewhat higher attenuation within the Iranian Plateau and low attenuation in the Arabian Plate and across the Caspian Sea. This is consistent with prior studies that suggest a hot and thin lithosphere beneath the Iranian Plateau. The Sn attenuation tomographic models at low frequency (0.3 Hz) and high frequency (2 Hz) are quite different. The biggest difference occurs in the northwestern Iran both within the plateau and the Zagros mountain belt. We observe a northeast-southwest directed finger of high Q that extends to the Alborz Mountains in the low frequency Sn Q model (Figure 24a), but this largely disappears in the high frequency Sn Q measurements. This difference might be due to the difference in propagation of the higher and lower frequency components of Sn. Alternatively, this difference could be due to difference in the uppermost mantle shear wave velocity gradient. We do not think that the crustal component or near site effects are dominant since we observe similar patterns in our RTM Sn Q model.

The strong frequency dependence can be explained by the high frequency Sn traveling more as a true head wave along the Moho and the low frequency Sn diving down to depths of 100 to 150 km in the uppermost mantle. Based on the results shown in Figure 25, we suggest that a hot and thin lithosphere beneath the Iranian Plateau and the Arabian Plate is underthrusting beneath the Eurasian Plate. This is consistent with both of our frequency dependent Q models.

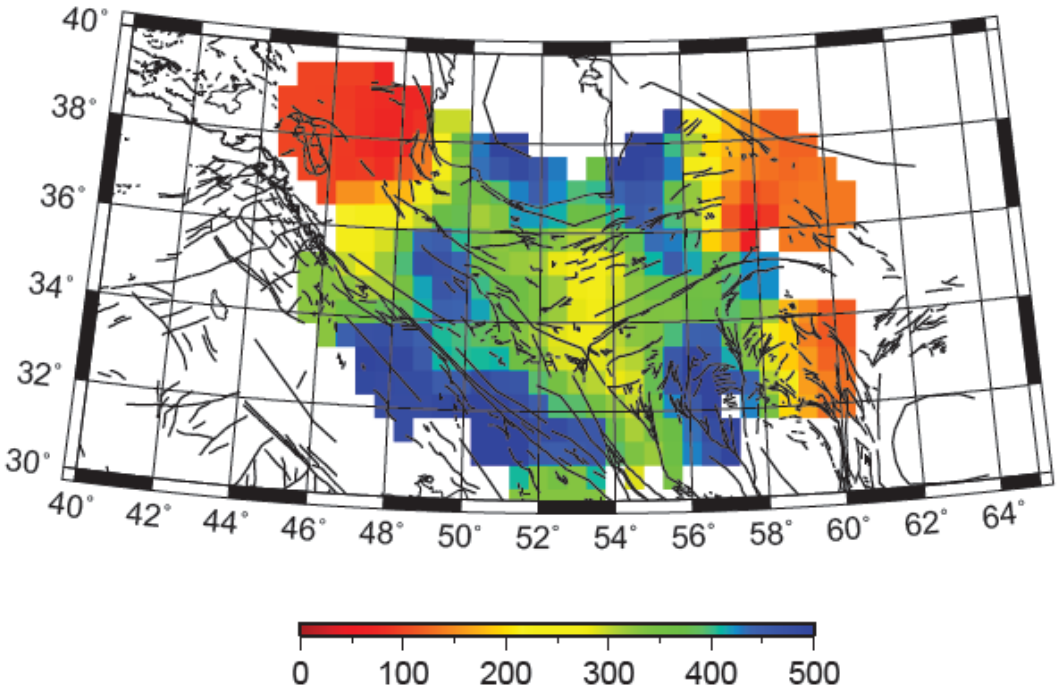

Figure 25. The reverse two station Sn Q tomographic model at 2 Hz for the Iranian plateau. We were able to extract approximately 3,000 reverse two station paths using about 12 years of data recorded in Iran.

We combined efficient and inefficient Sn measurements from events in southern Iran and the Caspian Sea in order to make more than 3000 RTM Sn Q measurements. As previously discussed, the RTM method should eliminate any site effects from the path

measurements. The RTM method may be even more important for Sn since there is a crustal component of the Sn wave path that could also contaminate the path measurements. Surprisingly, we have not found a large difference in Q models for Sn in Iran between the RTM and TSM methods. This does not appear to be the case in other tectonics provinces such as northern China, implying that for the Iranian plateau the differences in the near site terms and the crustal leg component of Sn attenuation are all secondary to the uppermost mantle path attenuation.

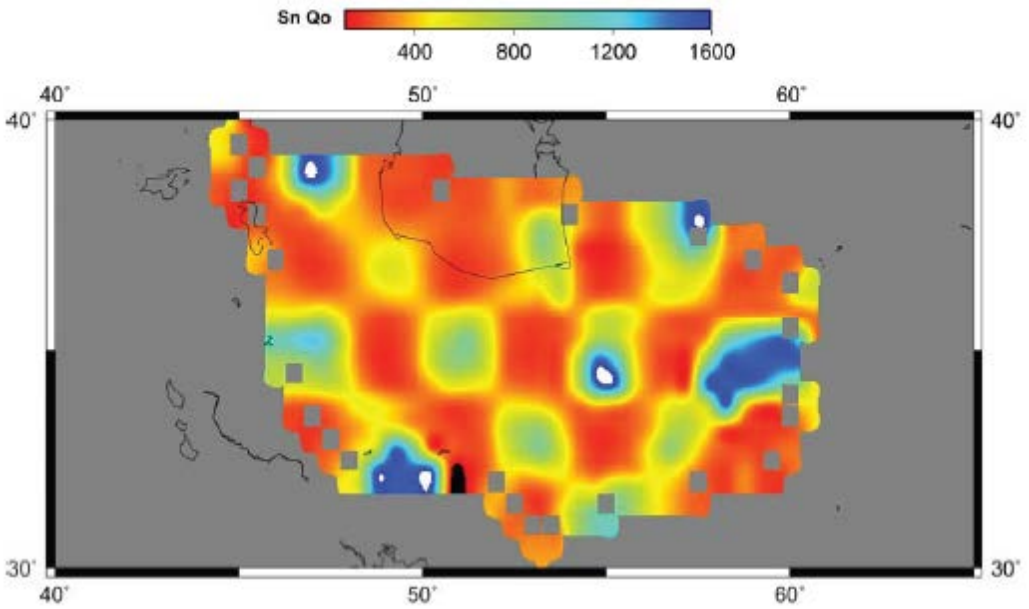

Figure 26. Checkerboard test for our Sn Q RTM tomographic model.

It is important to note that we have not yet fully incorporated some key aspects of regional phase propagation in our models such as regional phase conversions. Sn to Lg converted energy is likely to contaminate some of our measurements, especially from paths crossing the Caspian Sea. This is one likely explanation for the high Lg group velocities that we observe here (Figure 17). We have done our best to eliminate these effects by manually picking Sn travel time windows and not allowing energy below an uppermost mantle velocity of 4.3 km/s to contaminate our amplitude windows.

Another important problem is the large number of blocked paths, even for events larger than magnitude 4.5. It is important to note that we rarely observe Sn phase in Iran for events smaller than magnitude 4, possibly because the lower frequencies are not sufficiently excited and the higher frequencies attenuate over short distances. However, we still have a large number of blocked Sn paths that we are currently not incorporating into the model because they would overwhelm our TSM and RTM results. We plan to test weighting schemes to better incorporate this type of data in future work.

4.5 Pg Q Tomography

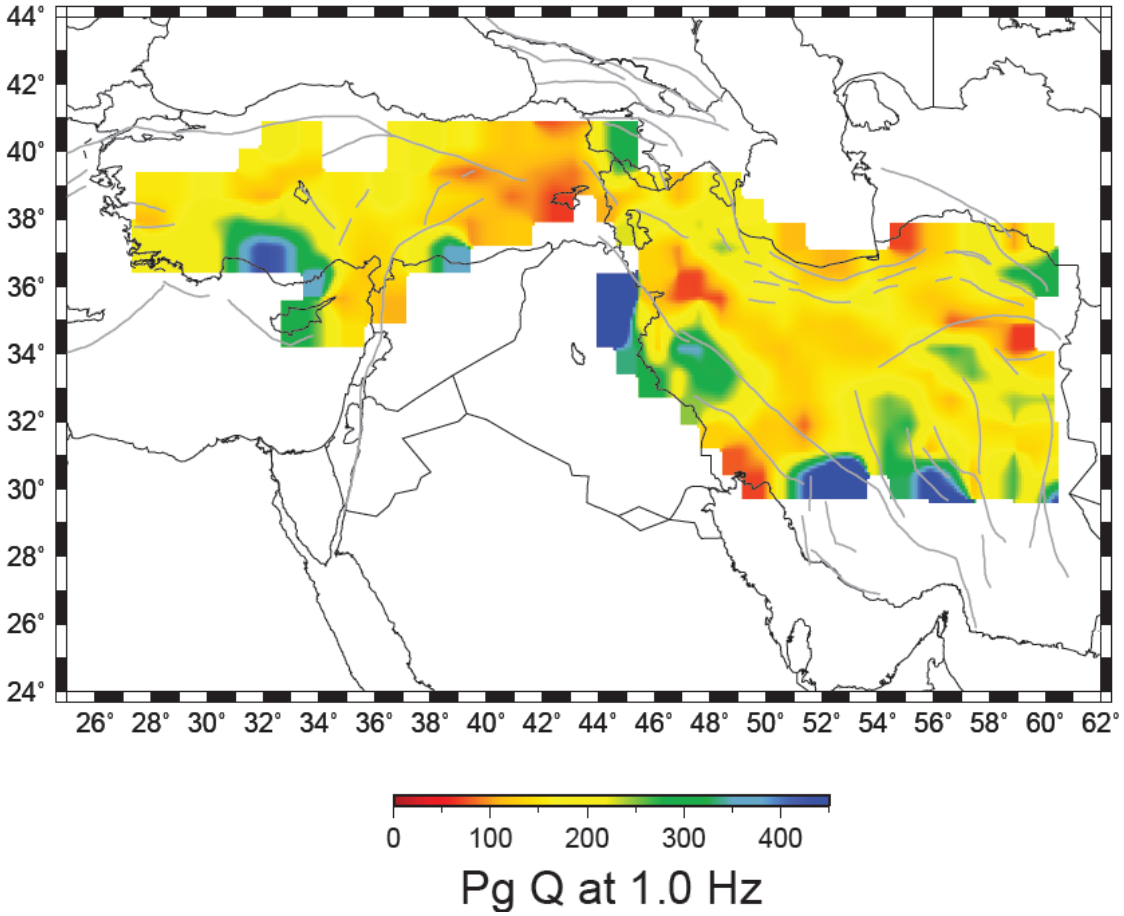

Figure 27. Our two station (TSM) for the regional phase Pg across the Iranian plateau.

We have also applied a two-station method to estimate Pg Q_0 (Q at 1 Hz) and the frequency dependence η using a relationship similar to what we used for Lg Q (Xie and Mitchell, 1990),

$$\ln\left(\frac{A_i(f)}{A_j(f)}\right) = -m\ln\frac{\Delta_i}{\Delta_j} + \frac{f^{1-\eta}}{Q_0}\frac{\pi\Delta_{i,j}}{V_{Pg}} \qquad (1)$$

Where V_{Pg} is the empirical Pg group velocity which we is typically around 5.6 km/sec and f is 1 Hz. Δ_i, Δ_j and $\Delta_{i,j}$ are the epicentral distance for each station and the inter-station distance respectively. A_i and A_j are Pg amplitudes for each station in frequency domain. By calculating the ratio of Pg spectra of two stations for each event and applying the instrument responses for each station, this method directly eliminates the source on the Pg spectrum. The amplitude ratio in frequency domain of two stations' waveforms for each event, represented in left term of equation (13), can be solved from spectrum of each station by separately picking the Pg window with the group velocity range from 6.1 km/sec to 5.1 km/sec. We set the maximum acceptable signal/noise ratio to 1.6 in this study as well as manually reviewing each regional seismogram to determine the Pg

propagation efficiency. We have used the same instrument response determined from our Lg study. We have also used the same geometric spreading as was used for Lg, however, we have also generated Q models using the Pg geometric spreading model of Bao et al., 20011b. The two-station method is still sensitive to the frequency bandwidth (Ford et al, 2008) possibly related to the influence from scattering attenuation, focusing/defocusing, and three-dimensional earth structures.

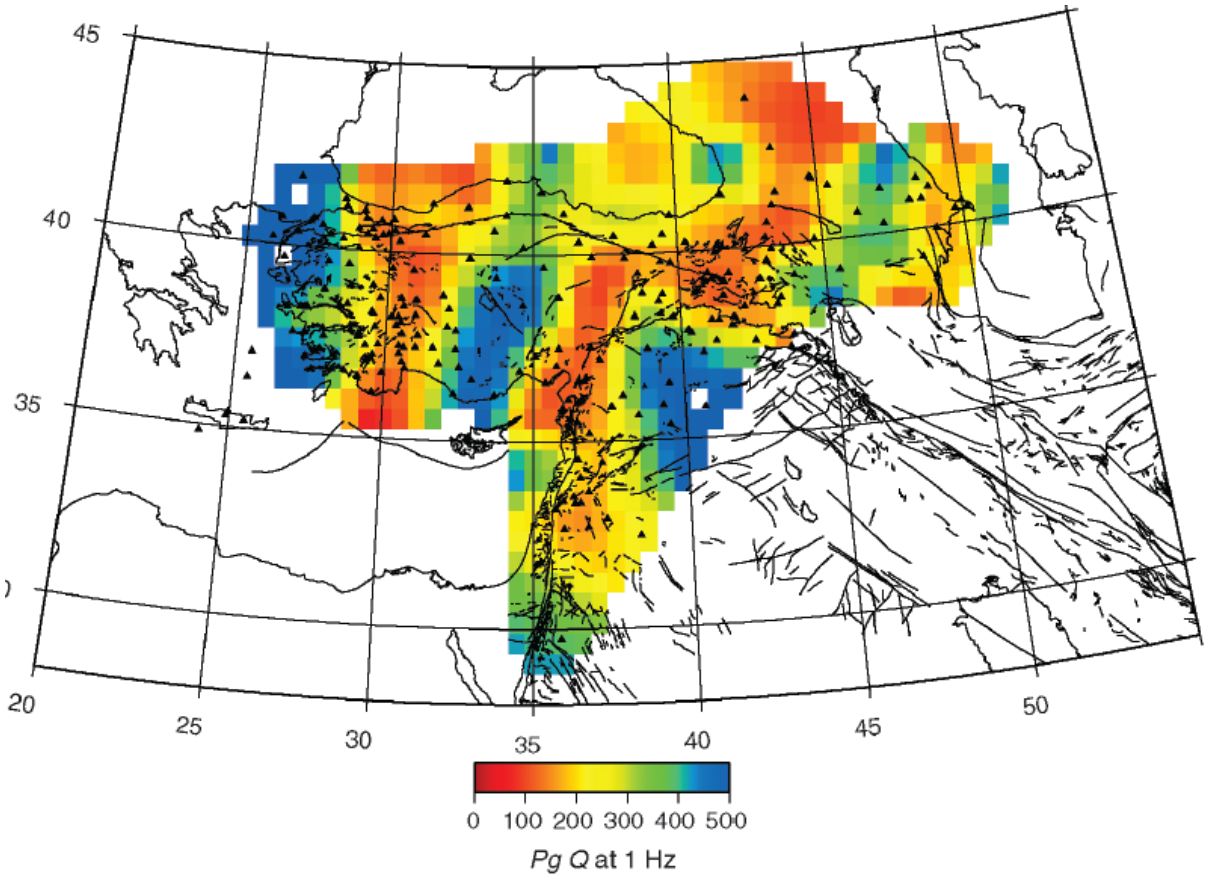

Figure 28. A tomographic image of Pg Q_0 lateral variation with 0.5° x 0.5° cell size in the northern Middle East. This model is from Bao et al, 2011b.

In general we observe fairly good correlation with our Lg Q map for the Iranian plateau. We observe high Q in the southeastern corner of the plateau and moderately low Q throughout the Zagros and western end of the plateau. One of the most surprising results from our initial Pg Q tomographic model is the relatively high Pg Q values that we have found within northwestern Iran, which is not consistent with the very low Q values we have found for Lg and Sn in this region. Since this region is at the edge of our model, the morphology of the high Q anomaly might be distorted by the ray coverage in this region. Examining an earlier model of Pg attenuation by Bao et al., 20011b (Figure 28), we also observe some evidence of a high Q anomaly in northwestern Iran. In the future we plan to combine all of the Pg measurements of Bao et. al., 2011b with our measurements for the Iranian plateau. This combined data set should provide us excellent coverage of the entire northern Middle East.

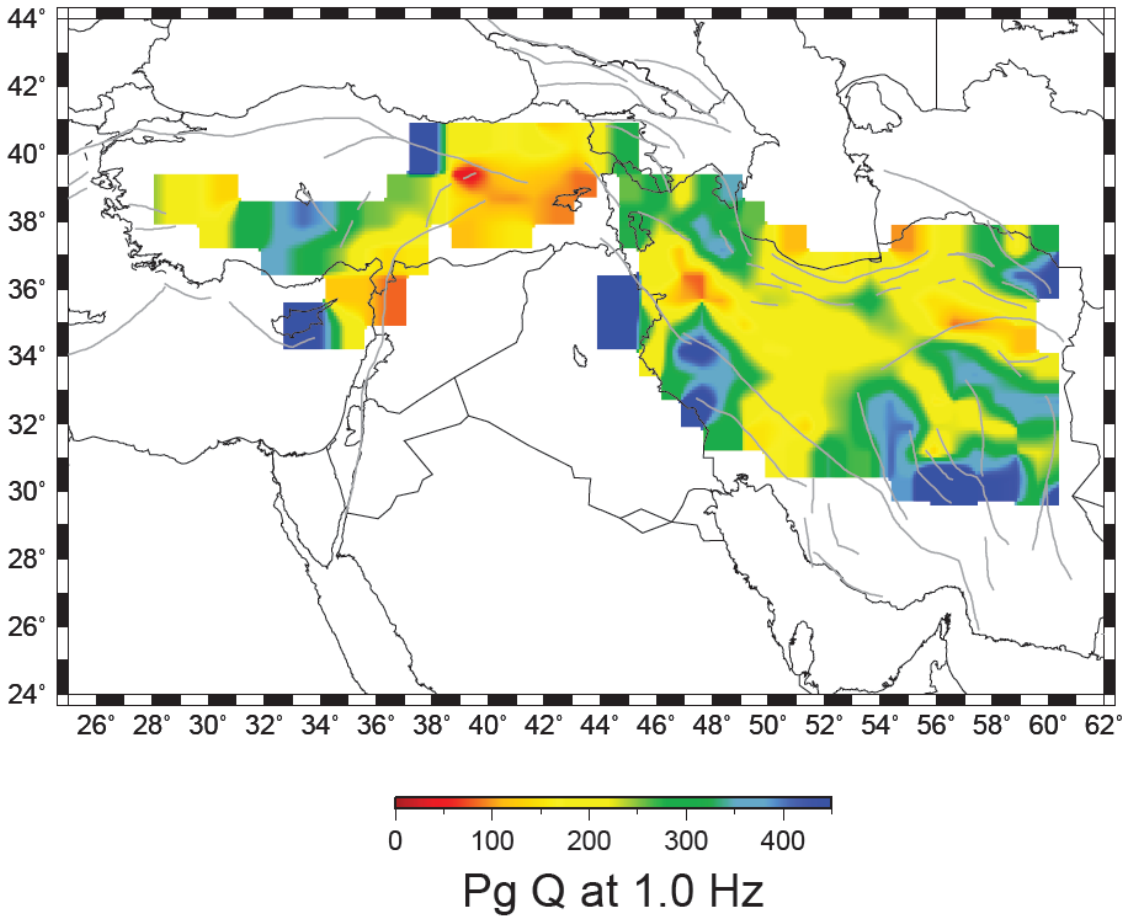

Figure 29. Our two station (RTM) for the regional phase Pg across the Iranian plateau.

We have also utilized the RTM method to map variations in Pg Q. The method is identical to what we used for Lg, only the group velocity, distance range, and the automated quality control parameters are different (e.g. a lower signal to noise ratio was used). When comparing the TSM and RTM Pg Q models we observe relatively similar structures across the Iranian plateau. The TSM versus RTM Pg Q models are relatively different within the Anatolian plateau, however, our ray coverage for the RTM Pg Q model is not very good within Anatolia. In the future we expect to improve the RTM coverage from ongoing seismic experiments in this part of the Anatolian plateau.

We also observe significant differences in Anatolia when comparing with the published model of Bao et al, 2011b. These differences are at least partly due to the fact that Bao et al., 2011b, used a geometric spreading exponent of 1.3 rather than 0.5 (which is spreading exponent that was used in Figures 27 and 29). We do consistently observe very high Q values in central Anatolia; something that is commonly observed with Pg propagation.

4.6 Characterizing coda across the Iranian plateau

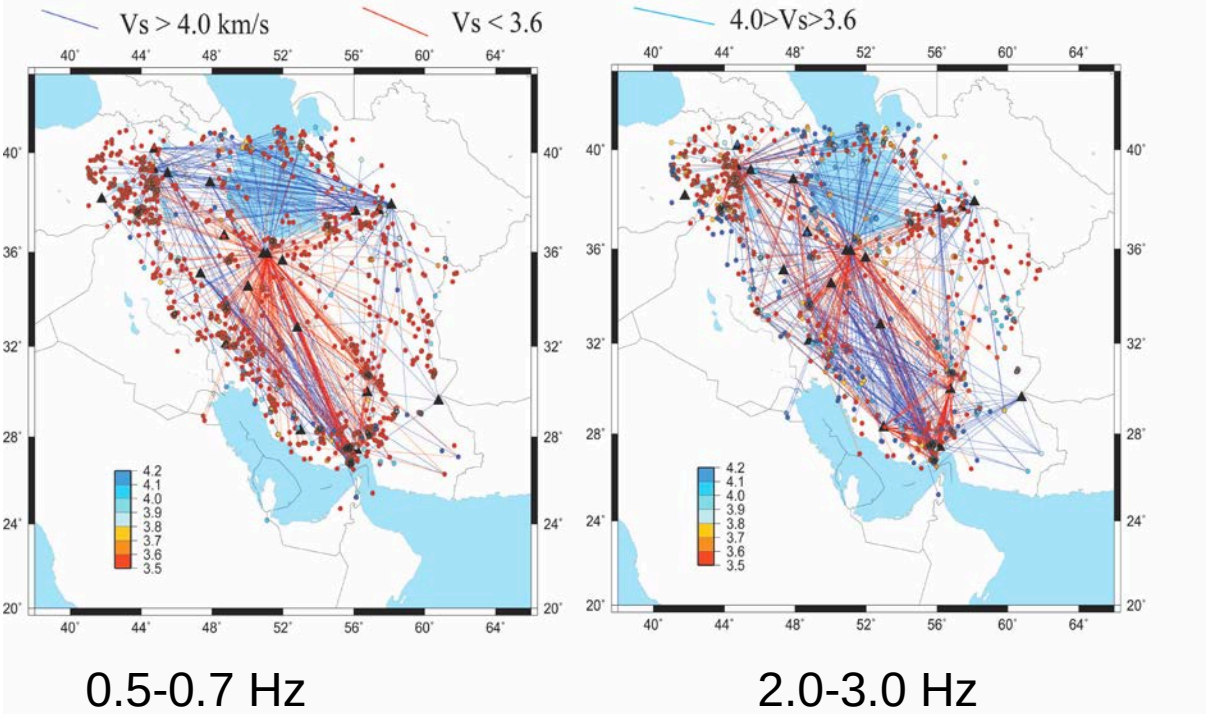

Figure 30. A ray path map showing the systematic variations in coda velocities for regional paths across the Iranian plateau. It is interesting to note that these are fairly consistent with variations in Lg peak group velocity.

In addition to studying direct phase amplitudes, we have also measured properties of regional coda across the Iranian plateau. We have used all of the same data from our work on Lg, Sn and Pg to measure different aspects of coda in order to construct a database of reliable source spectra for the Iranian plateau. Future work will allow us to compare Q values obtained from source corrected amplitude spectra. In addition to this, we have begun picking Pg windows and efficiencies.

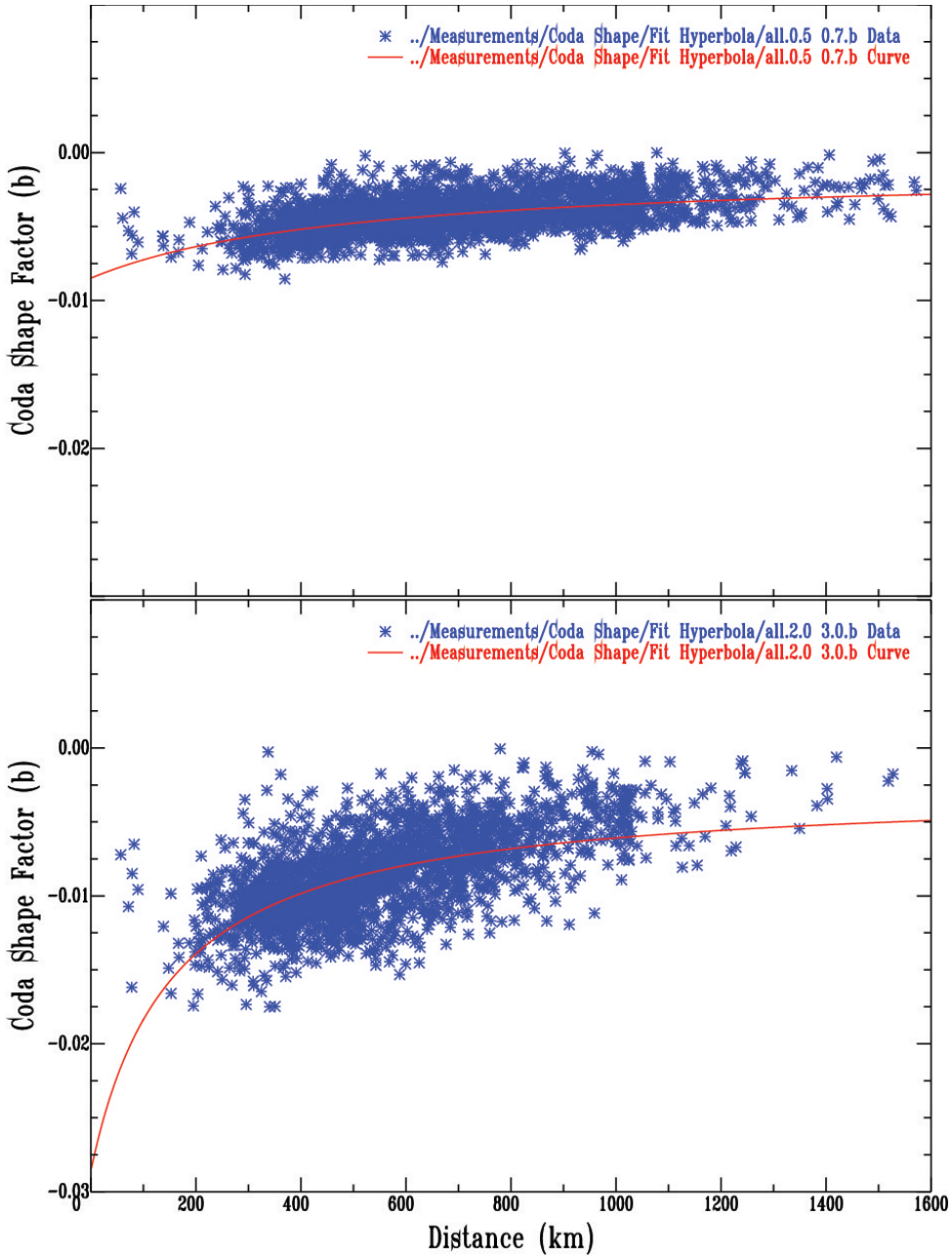

Figure 31. A plot of coda shape factors after regional 1D corrections have been applied (top) and before (bottom). Note the reduction in scatter as a function of distance.

In order to better characterize source characteristics to improve attenuation models, we used the empirical technique of Mayeda et al., 2007, to measure coda parameters for the Iranian plateau. We mapped variations in these parameters as a function of path (e.g., Vs for 0.5 to 0.7 and 2.0 to 3.0 Hz). Figure 30 illustrates the need for 2D corrections for higher frequency coda (note the substantial scatter remaining in the top plot). This also implies that 2D corrections will be necessary to characterize smaller sources with coda; however, we have found that the 1-D correction developed in this study led to reasonably robust coda magnitude values (see Figure 31).

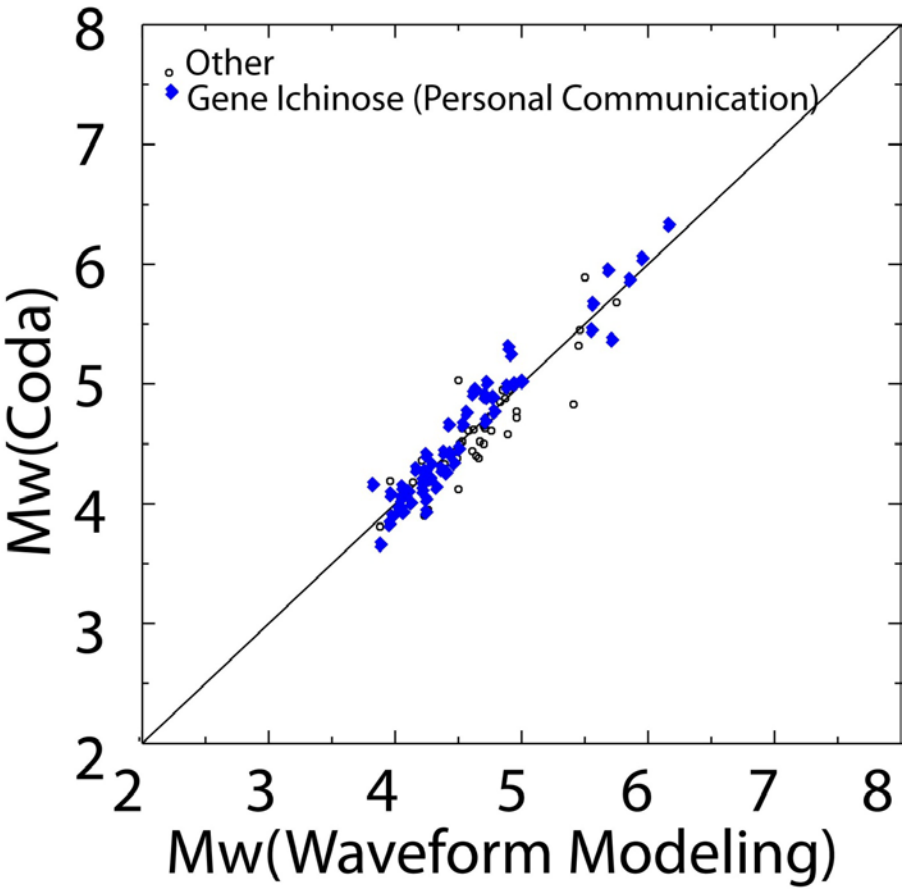

Figure 32. A plot of coda magnitude versus Mw. The coda magnitudes were calculated from the 1-D corrections determined in this study.

5. CONCLUSIONS AND RECOMMENDATIONS

5.1 Model Interpretations

Similar to Q, the shear wave velocity anomalies in the crust also have two primary causes: composition and temperature. Temperature anomalies in the crust should lead to a reduction in both Q and velocity; however, compositional or scattering anomalies should not necessarily produce a strong correlation in velocity and attenuation. By merging velocity and attenuation structure, we can distinguish between compositional and temperature anomalies as the source of the observed seismic structure. To that end, we present a very reliable model of frequency dependent Lg Q with relatively high resolution, which can serve as a proxy for bulk Qs of the crust. We also present an Lg group velocity model that is very well correlated with the Lg Q model. These two models, when combined, present a uniquely well constrained view of the crust in the northern Middle East.

Lg Q_0 and η are computed between pair of stations (and events) using Two-Station (TSM) and Reverse Two Stations/Events (RTM) geometries. The Lg Q_0 and η values measured over individual TSM and RTM paths are then inverted to obtain regionalized tomographic models of Lg Q0 and η. Lg group velocity model is obtained by inverting the first arrival time of the Lg waveform on each seismogram. The Lg Q model presented in our study is consistent with previous studies but with more reliable Q estimates, from the RTM method, and higher resolution within the Iranian plateau. As expected, we observe relatively low Q_0 values along the Arabian-Eurasian plate boundaries including the Anatolian and Iranian plateaus. Within this region, however, one of the more striking aspects of the model is the very low Q values ($Q < 70$) in easternmost Anatolia, along the border between Armenia and Turkey. In the past these absolute values might not have been considered reliable, but RTM provides reliable results, suggesting extremely high crustal attenuation. These anomalies are present in both the RTM and TSM models (Figures 12 and 13). We observe a strong correlation between our Lg Q and velocity models in that the regions presenting relatively low Q_0 are characterized by low Lg velocities and the regions showing high Lg Q_0 also show high Lg velocities. We observe very low Q and relatively low group velocities in Eastern Turkey, which is suggestive of a significant amount of partial melt in the crust. We also observe a relatively strong correlation between active volcanism and these anomalies. Furthermore, there is very weak frequency dependence in this same region, which is suggestive of intrinsic attenuation being the dominant mechanism of Lg blockage across this region. Igneous rocks tend to get younger towards the eastern part of the Bitlis suture and Kars plateau (e.g. Keskin, 2003), which is consistent with the largest amount of partial melt being in the easternmost Anatolian crust.

One of the regions where there is not a positive correlation between attenuation and velocity is the eastern Mediterranean. The strong negative correlation that we observe can be explain by the presence of a true oceanic crust which typically blocks Lg (leading to a very low Q) and a mafic composition leading to a relatively large shear wave velocity.
Surprisingly, we have not found extremely low Q values within the Zagros fold and thrust belt. This suggests that the well-known blockage of Lg across this region (e.g. Sandvol et al., 2001; Baumgardt, 2001; Kadinsky-Cade, 1981) is the result of scattering attenuation at the eastern terminus of the Mesopotamian Foredeep (MF) and not the crustal root beneath the Zagros. This idea is consistent with our TSM model that shows a very abrupt decrease in Lg Q at edge of the MF as well as the relatively strong frequency dependence of our Q values within the Zagros Fold and Thrust belt. The strong frequency dependence of Lg Q here is consistent with scattering attenuation being the dominant mechanism for Lg attenuation across this region. Furthermore, we see little change in Lg Q or its frequency dependence across much of the Iranian plateau. This is suggestive of few major changes in crustal structure or sediment thickness across much of the Iranian plateau. The lone exception is the region between the central Zagros and the Lut block.
The Q values in the central portion of the Iranian plateau, between the central Zagros and the Lut block, are significantly higher than the surrounding plateau. This region is also characterized by relatively Lg high group velocities. In fact, throughout the Iranian plateau we observe no region with Q values lower than 150 except for the northwestern-most Iranian plateau. The region with the highest Q value, close to 400, has relatively

thin sedimentary cover; this might be the reason for the relatively higher Q values here. Alternatively this tectonic region may be a separate crustal block that has had relatively little internal deformation and has a relatively uniform crustal wave guide. The coincidence of relatively higher Lg Q0 and group velocities beneath the Central Iranian blocks implies that the crust is likely far from partial melting. This suggests that the subcrustal mantle is in a lower-than-solidus temperatures state as also suggested by Kaviani et al. (2007). Furthermore our results imply that there could be significant far-field impacts to large earthquakes in the Makran, Zagros or Iranian plateau, because Lg is not strongly attenuated in these regions.

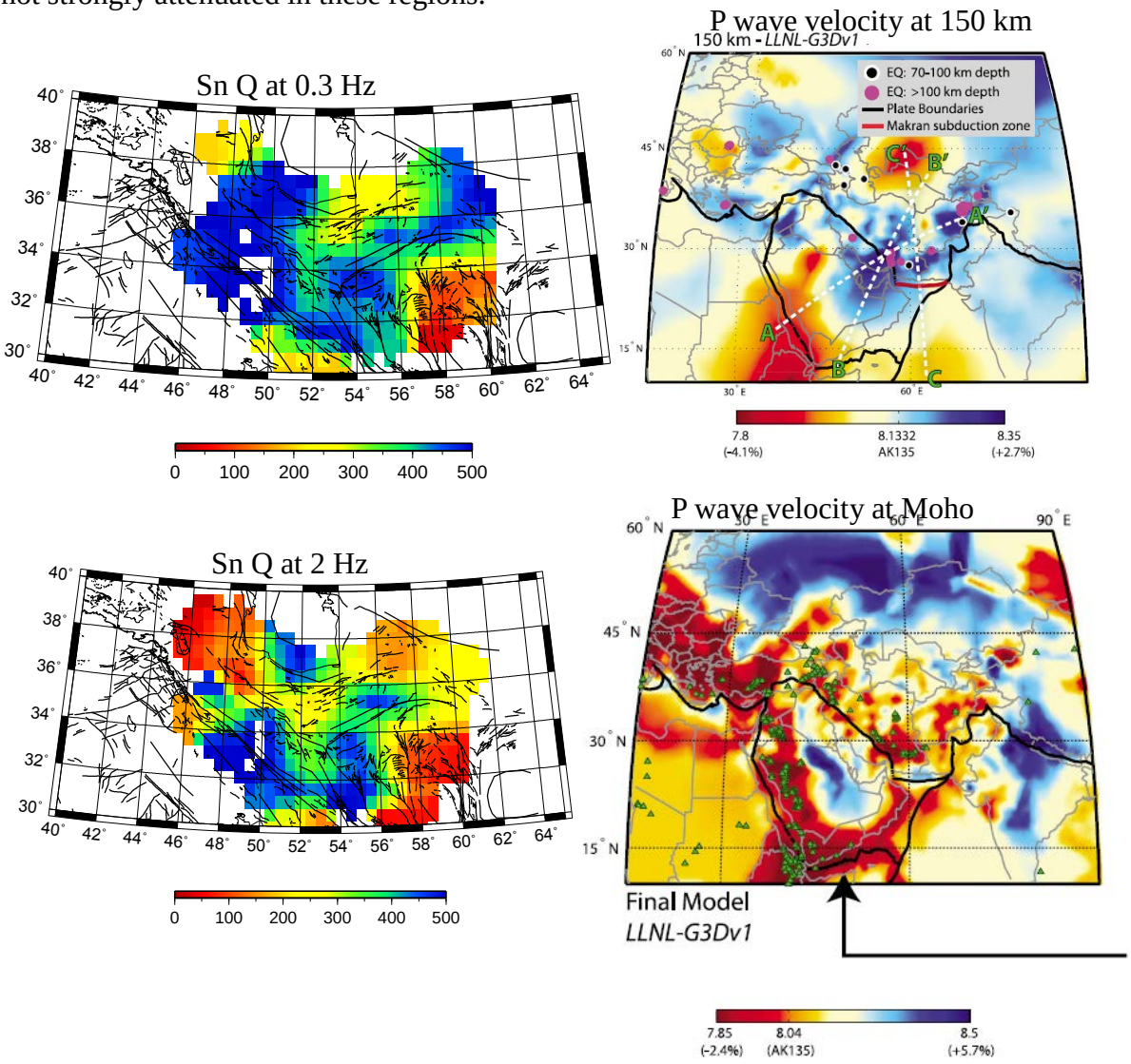

Figure 33. A comparison of upper mantle P-wave velocities and Sn Q values using the model of Simmons et al., 2012. We observe some evidence that our frequency dependence corresponds with a high velocity body that underlies the Iranian plateau at about 150 km depth. It may be possible that lower frequency Sn waves are traveling through this higher Q and Vs body.

It is important to note that we do not observe a significant change in Lg Q across the Zagros Mountains. This is not necessarily consistent with previous work that has shown that in general Lg is blocked across the portion of the Arabian-Eurasian plate boundary (e.g. Kadinsky-Cade et al., 1981; Rodgers et al., 1997; Sandvol et al., 2001). The lack of a clear change in Lg Q across the Zagros may be a result of our two station path azimuthal coverage being mainly restricted to paths that travel parallel to the strike of the mountain belt. If the dominant mechanism for Lg blockage is scattering caused by variations in crustal structure (i.e. thickness, sedimentary basins, etc.) then our results are most likely consistent with this idea because very few of the two station paths cross the entire mountain belt. Furthermore, the relatively strong LgQ frequency dependence implies that the scattering attenuation mechanism is strong in this region.

The observed relatively high Q values for the southern edge of the Caspian Sea are probably the result of very efficient Lg propagation through the Alborz Mountains. This observation has important implications for seismic hazard because even distant earthquakes are likely to produce strong ground motion within the Alborz Mountains. This also suggests that there is not a substantial crustal root that is sufficient to generate large amounts of scattering attenuation in this region.

The relative contribution of anelastic attenuation and scattering to the diminution of seismic energy is difficult to determine. Mitchell (1997) believes that the main cause of dissipation of seismic energy in the upper crust is the high intrinsic attenuation associated with the presence of aqueous fluids in the cracks. The presence of cracks is a determining factor in the attenuation of seismic waves in the upper crust by scattering related to the geometry of the cracks and by energy absorption through fluid movements along the cracks. The intrinsic attenuation in dry rocks seems to be weakly frequency dependent and hence the frequency dependence of seismic attenuation may be most likely related to the presence of fluids in rocks and cracks (e.g., Toksöz et al., 1990) and scattering of seismic waves (Dainty, 1981). In the regions where we observe low Q and low frequency dependence, we may infer dry crustal material with strong intrinsic attention.

Unlike our Lg Q model, our Sn Q model shows fairly strong frequency dependence, especially within the Iranian plateau itself. We observe this frequency dependence in both the RTM and TSM methods and thus it appears unlikely that this is caused by crustal components of Sn attenuation (consistent with our Lg Q models) or near site effects on Sn (also consistent with our Lg site terms). This suggests that something is happening with the path based attenuation of the Sn phases. We may be observing two different modes of propagation for Sn: high frequency head wave traveling at or near the Moho and diving shear waves that penetrate deeper into the upper mantle. There is evidence from velocity tomography that there is a high velocity and possibly higher Q body beneath Iran that may allow for more efficient propagation of diving S waves at regional distances.

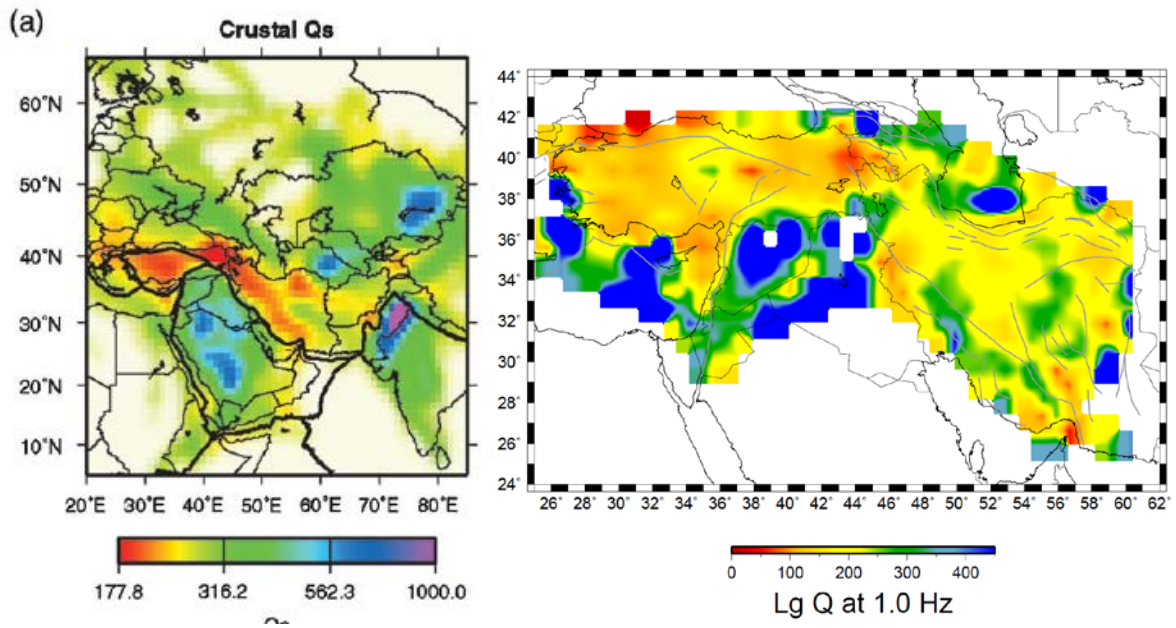

Figure 34. A comparison of the crustal Qs model of Pasyanos et al., 2009, and our Lg Q model at 1 Hz for the northern Middle East.

5.2 Model Comparisons

One method for circumstantially determining the reliability of the different methods applied to determine regional phase Q is the comparison of completely independent techniques. This comparison is useful because the models presented here are unlikely to be the 2-D or 3-D models incorporated into the MDAC, so it is important to note where there are differences in the models and understand the origin of those differences. Figures 36 and 34 shows that there is generally fairly good agreement between the amplitude based tomography and our Q tomography using TSM and RTM methods. This is a positive sign but we do observe differences in the details between the models and it is unclear whether these smaller features are robust given the substantial amount of noise that can be caused by phase conversions (e.g. Sn to Lg), anisotropic scattering attenuation, and possible azimuthal variations in site amplification. Site amplifications are another important portion of our models that should be compared with the amplitude tomography approach. It is important to note that the reverse two station site amplification is a fundamentally different measure of site amplification because, in theory, it should not be a function of ray path coverage or density of events and stations. Nevertheless, we observe site terms with orders of magnitude (-1.5 to 1.5) that are similar to those observed using other techniques in other regions.

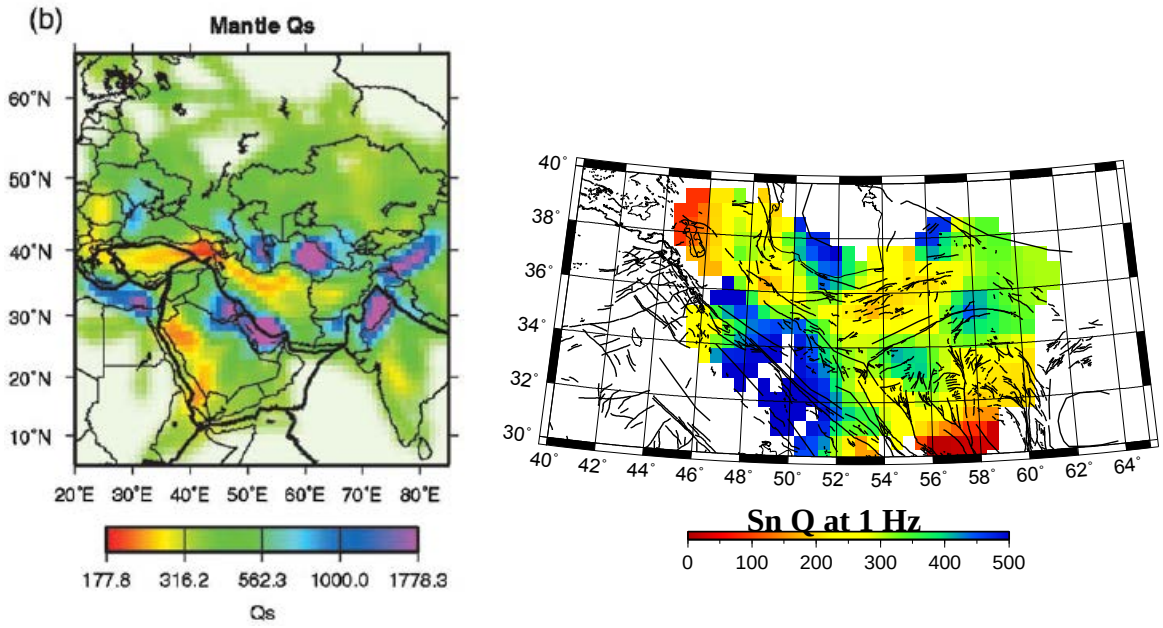

Figure 35. A comparison of the mantle Qs model of Pasyanos et al., 2009 and our Sn Q model 1 Hz for the northern Middle East.

Our Sn Q model is comparable to the upper mantle Qs model from Pasayanos et al. (2009) for the Iranian plateau although substantially less smooth than the Pasayanos (Figure 35). It may be useful to examine a tomographic model from a much larger data set in order to better understand the level of complexity of the uppermost mantle beneath the northern Middle East. When examining the Pn tomographic model of Amini et al. (Figure 34), 2012 we see significant small scale complexity in the uppermost mantle P-wave velocities especially beneath Iran. This would suggest that it is likely that the attenuation structure for Sn would be similarly complex because both anelasticity and scattering attenuation are directly or empirically related to seismic velocity variations. Furthermore, if we compare the observed velocity variations in the Pn tomographic model to our Sn we observe some fairly good correlation between low Pn velocities with lower values of Sn Q (Figure 36). How important these smaller scale Q anomalies are to predicting amplitudes successfully depends a good deal on what the true amplitude of the Q anomalies are.

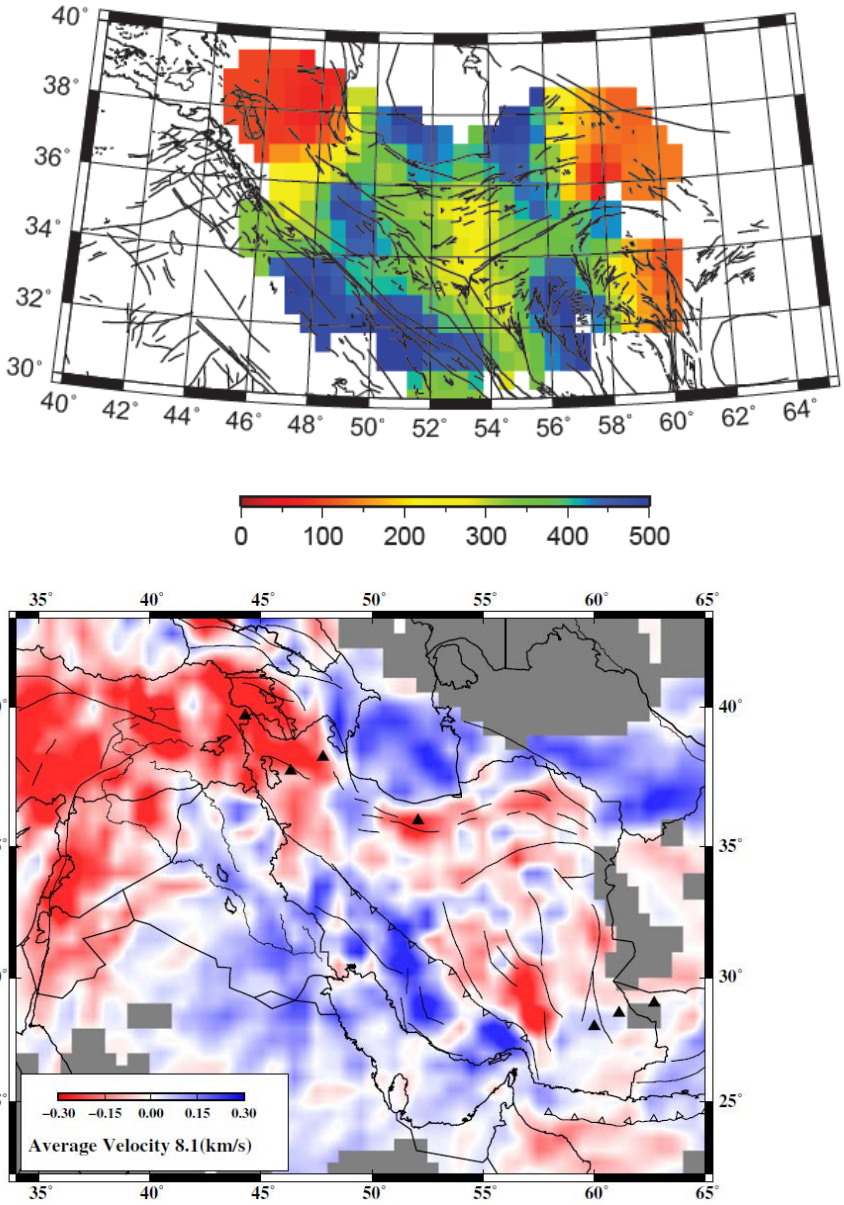

Figure 36. A comparison of the uppermost mantle Qs model using Sn RTM Q values and Pn tomography of Amini et al., 2012. The large scale anomalies are reasonably well correlated with Pn velocity. This could suggest that our Sn amplitudes are most strongly affected by anelasticity of the uppermost mantle or Vs velocity gradients which would probably also correlate with Pn velocity.

Future work needs to focus on how the propagation of Sn and the effect of different distances and uppermost mantle shear wave velocity gradient has on the scattering of Sn waves and the nature of the frequency dependence of the scattering attenuation of Sn. The fact that we observe strong frequency dependence of Sn Q suggests that scattering plays a key role in the attenuation of Sn in the Iranian plateau.

REFERENCES

Al-Damegh K., E. Sandvol, A. Al-Lazki, and M. Barazangi, Regional Seismic wave propagation (Lg and Sn) and Pn attenuation in the Arabian Plate and surrounding regions, *Geophys. J. Int.*, 157, pp. 775-795, 2006.

Al-Lazki, A. I., D. Seber, E. Sandvol, N. Turkelli, R. Mohamad, and M. Barazangi, Tomographic Pn velocity and anisotropy structure beneath the Anatolian plateau (eastern Turkey) and the surrounding regions, *Geophys. Res. Let*. 30, (24), 2003.

Amini, S., Z. H. Shomali, H. Koyi, and R. G. Roberts, Tomographic upper-mantle velocity structure beneath the Iranian Plateau, *Tectonophysics*, 554-557, pp. 42-49, 2012.

Bao, X., E. Sandvol, J. Ni, T. Hearn, Y. J. Chen, and Y. Shen, High resolution regional seismic attenuation tomography in eastern Tibetan Plateau and adjacent regions, *Geophys. Res. Lett*., 38, L16304, doi:10.1029/2011GL048012, 2011a.

Bao, X., E. Sandvol, E. Zor, S. Sakin, R. Mohamad, R. Gök, R. Mellors, T. Godoladze, G. Yetirmishli, and N. Türkelli, Pg attenuation tomography within the northern Middle East, Bull. Seismol, *Soc. Am.*, Vol. 101, No. 4, pp. 1496-1506, August 2011, doi: 10.1785/0120100316, 2011b.

Bao, X., E. Sandvol, Y. J. Chen, J. Ni, T. Hearn, and Y. Shen, Azimuthal anisotropy of Lg attenuation in eastern Tibetan Plateau, *J. Geophys. Res.*, 117, B10309, doi:10.1029/2012JB009255, 2012.

Barron, J. and K. Priestley, Observations of frequency-dependent Sn propagation in Northern Tibet, *Geophysical Journal International*, 179 (1), pp. 475-488, 2009.

Baumgardt, D. R., Sedimentary basins and the blockage of Lg wave propagation in the continents, *Pure and Appl. Geoph*., 158, pp. 1207-1250, 2001.

Berberian, M. and G. C. P. King, Towards a Paleogeography and tectonic evolution of Iran, *Canadian Journal of Earth Sciences*, 18, pp. 210-265, 1981.

Berberian, M., Master "blind" thrust faults hidden under the Zagros folds: Active basement tectonics and surface morphotectonics, *Tectonophysics*, 241, pp. 193-224, 1995.

Bouchon, M. The Complete Synthesis of Seismic Crustal Phases at Regional Distances, *J. Geophys. Res*. 87, pp. 1735-1741, 1982.

Campillo, M., Propagation and attenuation characteristics of the crustal phase Lg, *Pure Appl. Geophys*., 132, pp. 1-19, 1990.

Chun, K.-Y., G. F. West, R. J. Kokoski, and C. Samson, A novel technique for measuring *Lg* attenuation; results from Eastern Canada between 1 to 10 Hz, *Bull. Seismo. Soc. Amer*., 77, (2), pp. 398-419, 1987.

Cong, L. and B. Mitchell, Lg coda Q and its relation to the geology and tectonics of the Middle East, *Pure appl. Geophys*, 153, 2-4, pp. 563-585, 1998.

Coleman R. J., (ed.), Oman Ophiolites. *Journal of Geophysical Research* (Special Issue) 86, pp. 2495-2782, 1981.

Dainty, A. M., A scattering model to explain seismic Q observations in the lithosphere between 1 and 30 Hz, *Geophys. Res. Lett.*, 8, pp. 1126–1128, doi: 10.1029/GL008i011p01126, 1981.

Der, Z. A., M. E. Marshall, A. O'Donnell, and T. W. McElfresh, Spatial coherence structure and attenuation of the *Lg* phase, site effects, and the interpretation of the *Lg* coda, *Bull. Seismol. Soc. Am*., 74, pp. 1125-1147, 1984.

Dewey, J.F. and J. M. Bird, Mountain bets and the new global tectonics, *Journal of Geophysical Research*, 75, pp. 2625-2647, 1970.

Fan, G. W. and T. Lay, Strong Lg wave attenuation in the Northern and Eastern Tibetan Plateau measured by a two-station/two-event stacking method, *Geophysical Research Letters*, 30 (10), pp. 37-1, 2003.

Ford. S. R., D. S. Dreger, K. Mayeda, W. R. Walter, L. Malagnini, and W. S. Phillips, Regional Attenuation in Northern California: A Comparison of Five 1D *Q* Methods, *Bull. Seism. Soc. Am.*, 98: pp. 2033-2046, 2008.

Ghazi, A.M., E. A. Pessagno, A. A. Hassanipak, S. M. Kariminia, and K. A. Campbell, Tectonogenesis of the Khoy ophiolite, NW Iran: Results from 40Ar-39Ar and biostratigraphic/chronostratigraphic, *International Conference on Geology of Oman, Muscat, Oman,* Abstract Volume, p. 48, 2001.

Gök, R., N. Turkelli, E. Sandvol, D. Seber, and M. Barazangi, Regional wave propagation in Turkey and surrounding regions, *Geophys. Res. Let*., 27, Issue 3, pp. 429-432, 2003.

Gök, R., L. Hutchings, K. Mayeda, and D. Kalafat, Source Parameters for 1999 North Anatolian Fault Zone Aftershocks, *Pure & Appl. Geoph*., 10.1007/s00024-009-0461, 2010.

Jackson, J. and D. McKenzie, Active tectonics of the Alpine-Himalayan Belt between western Turkey and Pakistan, *Geophys. J. R. astr. Soc.*, 77, pp. 185-264, 1984.

Kadinsky-Cade, K., M. Barazangi, J. Oliver, and B. Isacks, Lateral variations of high-frequency seismic wave propagations at regional distances across the Turkish and Iranian plateaus, *J. Geophys. Res*., 86, pp. 9377–9396, 1981.

Kaviani A., A. Paul, E. Bourova, D. Hatzfeld, H. Pedersen, and M. Mokhtari, A strong seismic velocity contrast in the shallow mantle across the Zagros collision zone (Iran), *Geophy. J. Int.*, 171, pp. 399-410, doi: 10.1111/j.1365-246X.2007.03535.x, 2007.

Kennett, B. L. N., Guided wave propagation in laterally varying media - I. Theoretical development. Geophysical Journal of the Royal Astronomical Society, 79: pp. 235-255. doi: 10.1111/j.1365-246X.1984.tb02853.x., 1984.

Keskin, M., Magma generation by slab steepening and breakoff beneath a subduction-accretion complex: An alternative model for collision-related volcanism in Eastern Anatolia, Turkey, *Geophys. Res. Lett.*, 30, 8046, doi:10.1029/2003GL018019, 24., 2003.

Knopoff, L., F. Schwab, and E. Kausel, Interpretation of Lg, *Geophys. J. R. Astron. Soc.*, 33, pp. 389-404, 1973.

Lippard S. J., A. W. Shelton, and I. G. Gass, The ophiolite of Northern Oman, *Geological Society of London Memoir*, 11, 178, 1986.

Maggi, A., J. A. Kackson, K. Priestley, and C. Baker, A re-assessment of focal depth distributions in southern Iran, the Tien Shan and northern India: Do earthquakes really occur in the continental mantle?, *Geophys. J. Int*., 143, pp. 629-661, 2001.

Mayeda, K., S. Koyanagi, M. Hoshiba, K. Aki, and Y. Zeng, A comparative study of scattering, intrinsic, and coda Q^{-1} for Hawaii, Long Valley, and central California between 1.5 and 15.0 Hz, *J. Geophys. Res.*, 97(B5), pp. 6643–6659, doi: 10.1029/91JB03094, 1992.

Mayeda, K., L. Malagnini, and W. R. Walter, A new spectral ratio method using narrow band coda envelopes: Evidence for non-self-similarity in the Hector Mine sequence, *Geophysical Research Letters*, 34 (11), art. no. L11303, 2007.

Meunier, P., N. Hovius, and J. A. Haines, Topographic site effects and the location of earthquake induced landslides, *Earth Planet. Sci. Lett.*, 275, pp. 221-232, doi: 10.1016/j.epsl.2008.07.020, 2008.

McClusky, S., S. Balassanian, A. Barka, C. Demir, S. Ergintav, I. Georgiev, O. Gurkan, M. Hamburger, K. Hurs, H. Kahle, K. Kastens, G. Kekelidze, R. King, V. Kotzev, O. Lenk, S. Mahmoud, A. Mishin, M. Nadariya, A. Ouzounis, D. Paradissis, Y. Peter, M. Prilepin, R. Reilinger, I. Sanli, H. Seeger, A. Tealeb, M. N. Toksoz, and G. Veis, Global positioning system constraints on plate kinematics and dynamics in the eastern Mediterranean and Caucasus, *Journal of Geophysical Research*, 105, pp. 5695-5719, 2000.

Michard A., J. L. Bouchez, and M. Ouazzani-Touhami, Obduction-related planner and linear fabrics in Oman, *Journal of Structural Geology*, 6, pp.39-49, 1984.

Mitchell, B. J., L. Cong, and G. Ekström, A continent-wide map of 1-Hz Lg coda Q variation across Eurasia and its relation to lithospheric evolution, *Journal of Geophysical Research B: Solid Earth*, 113 (4), art. no. B04303, 2008.

Mitchell, B. J., Frequency dependence of shear wave internal friction in the continental crust of eastern North America, *J. Geophys. Res.*, 85, pp. 5212-5218, 1980.

Mitchell, B., *Lg* coda Q variation across Eurasia and its relation to crustal evolution, *J. Geophys. Res* 102, (10), pp. 22,767-22,779, 1997.

Moorse, E. M. and F. Vine, The Troodos massif, Cyprus and other ophiolites as oceanic crust: evaluation and complications, *Transaction of Royal Society of London*, 268, pp. 433-466, 1971.

Molnar, P. and J. Oliver, Lateral variations of attenuation in the upper mantle and discontinuities in the lithosphere, *J Geophys Res*, 74 (10), pp. 2648-2682, 1969.

Mottaghi, A. A., M. Rezapour, and M. Korn, Ambient noise surface wave tomography of the iranian plateau, *Geophysical Journal International*, 193 (1), pp. 452-462, 2013.

Nuttli, O. W., Yield eastimates of Nevada Test Site explosions obtained from seismic *Lg* waves, *J. Geophys. Res.*, 91, pp. 2137-2151, 1986.

Paige, S. S. and M. A. Saunders, Algorithm 583, LSQR: Sparse linear equations and least-squares problems, *Trans Math Software*, 8**,** pp. 195-209, 1982.

Pasayanos, M. E., W. Walter, and E. Matzel, A Simultaneous Multiphase Approach to Determine P-Wave and S-Wave Attenuation of the Crust and Upper Mantle, *Bull. Seismo. Soc. Amer*., 99, (6), pp. 3314-3325, 2009.

Pessagno, E. A. and D. M. Hull, Upper Jurassic (Oxfordian) radiolaria from the Sula Islands (East Indies): Their taxonomic, biostratigraphic, chronostratigraphic, and paleobiogeographic significance, *Micropaleontology*, 48 (3), pp. 229-256, 2002.

Peters, T. J., A. Nicolas, and R. J. Coleman, (eds.), Ophiolite Genesis and evolution of the Oceanic Lithosphere. Proceedings of the Ophiolite Conference, held in Muscat, Oman, *Kluwer Academic Publisher*, 903, 1991.

Phillips, W. S., K. M. Mayeda, and L. Malagnini, Developments in regional phase amplitude tomography, *Seism. Res. Lett*., 80, p. 360, 2009.

Priestley, K., C. Baker, and J. Jackson, Implications of earthquake focal mechanism data for the active tectonics of the south Caspian Basin and surrounding regions, *Geophysical Journal International*, 118, pp. 111-141,1994.

Rodgers, A. J., J. F. Ni, and T. M. Hearn, Propagation characteristics of short-period Sn and Lg in the Middle East, *Bull. Seismo. Soc. Amer*., 87, (2), pp. 396-413, 1997.

Sandvol, E., K. Al-Damegh, A. Calvert, D. Seber, M. Barazangi, Mohamad, R, R. Gök, N. Turkelli, and C. Gurbuz, Tomographic imaging of Lg and Sn propagation in the Middle East, *Pure and Applied Geophysics*, 158, pp. 1121-1163, 2001.

Simmons, N. A., S. C. Myers, G. Johannesson, and E. Matzel, LLNL-G3Dv3: Global P wave tomography model for improved regional and teleseismic travel time prediction, *Journal of Geophysical Research B: Solid Earth*, 117 (10), art. no. B10302, 2012.

Stocklin, J., Structural history and tectonics of Iran; a review, *Bulletin of American Association of Petroleum Geologist*, 52 (7), pp. 1229-1258, 1968.

Talebian, M. and J. Jackson, Offset on the Main Recent Fault of NW Iran and implications for the late Cenozoic tectonics of the Arabia–Eurasia collision zone, *Geophys. J. Int.*, **150**, pp. 422-439, 2002.

Tchalenko, J. S. and J. Braud, Seismicity and structure of the Zagros (Iran): The Main Recent Fault between 33 and 35 degrees North, *Phil. Trans. R. Soc. A.*, 277, pp. 1-25, 1974.

Toksöz, M. N., B. Mandal, and A. M. Dainty, Frequency dependent attenuation in the crust, *Geophys. Res. Lett.*, 17, pp. 973-976, 1990.

Wald, D. J. and T. I. Allen, Topographic slope as a proxy for seismic site conditions and amplification, *Bull. Seismol. Soc. Am.*, 97, pp. 1379-1395, doi: 10.1785/0120060267, 2007.

Walter, W. and S. Taylor, A revised Magnitude Distance Amplitude Correction (MDAC2) procedure for regional seismic discriminants, Lawrence Livermore National Laboratory UCRL-ID-146882, 2002.

Xie, J. and B. J. Mitchell, Attenuation of multiphase surface waves in the Basin and Range province, Part I: *Lg* and *Lg* coda, *Geophys. J. Int.*, 102, pp. 121-137, 1990.

Xie, J., Source scaling of Pn, Lg spectra and their ratios from explosions in central Asia: Implications on identification of small seismic events at regional distances, *J. Geophys. Res.*, (B7), 10.1029/2001JB000509, 2002.

Xie, J., R. Gök, J. Ni, and Y. Aoki, Lateral variations of crustal seismic attenuation along the INDEPTH profiles in Tibet from *Lg Q* inversion, *J. Geophys. Res.*, 109, B10308, doi: 10.1029/2004JB002988, 2004.

Xie, J., Z. Wu, R. Liu, D. Schaff, Y. Liu, and J. Liang, Tomographic regionalization of crustal *Lg Q* in eastern Eurasia, *Geophys. Res. Lett.*, 33, L03315, doi: 10.1029/2005GL024410, 2006.

Zor, E., E. Sandvol, J. Xie, N. Türkelli, B. Mitchell, A. Gasanov, and G. Yetirmishli, Crustal attenuation within the Turkish plateau and surrounding regions, *Bull. Seismol. Soc. Am.*, 97, pp. 151-161, 2007.

LIST OF SYMBOLS, ABBREVIATIONS, AND ACRONYMS

AFRL	Air Force Research Laboratory
MDAC	Model Determined Amplitude Correction
RTM	Reverse Two Station Method
TSM	Two Station Method
KOERI	Kandilli Observatory and Earthquake Research Institute
IGTU	Institute of Geophysics, Tehran University
MZRF	Main Zagros Reverse Fault
IIEES	International Institute of Earthquake Engineering and Seismology
CIMB	Central Iranian Micro-Blocks

DISTRIBUTION LIST

DTIC/OCP
8725 John J. Kingman Rd, Suite 0944
Ft Belvoir, VA 22060-6218 1 cy

AFRL/RVIL
Kirtland AFB, NM 87117-5776 2 cys

Official Record Copy
AFRL/RVBYE/Robert Raistrick 1 cy